

Understanding Interquark Force and Quark Masses in Perturbative QCD*

Y. SUMINO

*Department of Physics, Tohoku University
Sendai, 980-8578 Japan*

Abstract

This lecture note presents a self-contained introduction to the theory of a heavy quark-antiquark ($Q\bar{Q}$) system in terms of perturbative QCD. The lecture is intended for non-experts, such as graduate course students. The heavy $Q\bar{Q}$ system serves as an ideal laboratory for testing various aspects of QCD: We can examine the nature of renormalons in perturbative series; an effective field theory Potential-NRQCD is constructed, whose derivation from full QCD can be traced stepwise; we see absorption of renormalons by non-perturbative matrix elements in OPE clearly; a systematic short-distance expansion of UV contributions can be performed, which predicts a “Coulomb+linear” potential in perturbative QCD; we can test these theoretical formulations by comparison to lattice computations, where we observe a significant overlap with perturbative regime; finally we can test our microscopic understanding by comparing to experimental data for the bottomonium states. These subjects are covered in a concise and elementary manner. Overall, we provide a microscopic description of the main dynamics of a heavy $Q\bar{Q}$ system, as an example for which theoretical framework, practical computations and qualitative understanding have been most advanced.

* Based on the lecture courses given at Rikkyo Univ., Kyoto Univ., Karlsruhe Univ. and Nagoya Univ., during 2012–2014.

Contents

1	Introduction	2
2	QCD Lagrangian, Chiral Symmetry, Quark Masses	4
2.1	Setup	4
2.2	Picture of spontaneous chiral symmetry breakdown	5
3	$\overline{\text{MS}}$ scheme and Running Coupling Constant	7
3.1	Renormalization and $\overline{\text{MS}}$ scheme	8
3.2	Renormalization group and running coupling constant	9
4	Interquark Force and QCD Potential	12
4.1	QCD potential from Wilson loop	12
4.2	Energy of a static quark pair	13
5	Renormalons in QCD Potential	16
5.1	Theoretical background: asymptotic series	16
5.2	Renormalons in $V_{\text{QCD}}(r)$: some details	17
6	Cancellation of Renormalons in Total Energy	21
6.1	Quark pole mass and total energy of $Q\bar{Q}$ system	21
6.2	Mechanism of cancellation of IR contributions	24
6.3	Perturbative prediction for $E_{\text{tot}}(r)$	26
7	“Coulomb+Linear” Potential by Log Resummation	29
7.1	Analysis of $V_{\text{QCD}}(r)$ in an EFT framework (Outline)	29
7.2	UV contributions to $V_{\text{QCD}}(r)$ and OPE	31
8	Implication and Interpretation	36
9	Potential-NRQCD EFT in Static Limit	39
9.1	Historical background	39
9.2	Basic concept of pNRQCD for static quarks	41
9.3	Derivation of Lagrangian and Feynman rules	42
9.4	Computation of $V_{\text{QCD}}(r)$ in pNRQCD	45
9.5	Matching to QCD	47
9.6	Renormalization of Wilson coefficient and μ_f -independence of $V_{\text{QCD}}(r)$	48
9.7	Renormalons in $V_{\text{IR}}(r)$	49
9.8	$V_{\text{QCD}}(r)$ at very small r and local gluon condensate	52
10	References for Further Studies	54
A	Formulas for Perturbative Series of $E_{\text{tot}}(r)$	59

B Computation of $V_C(r)$	61
C Integration-by-regions Method and Relation to EFT	62

1 Introduction

Studying properties of various hadrons has long been one of the standard analysis methods to elucidate the dynamics of the strong interaction. Among various observed hadrons, the heavy quarkonium states are unique, which are the bound states of a heavy quark-antiquark ($Q\bar{Q}$) pair. This is because they are the only known individual hadronic states whose properties can be predicted in a self-contained manner within perturbative QCD. Namely, we can compute several observables associated with individual heavy quarkonium states (such as energy levels, leptonic decay widths and transition rates) systematically in expansions in the strong coupling constant α_s . Such series expansions make sense, since the large mass of the heavy quarks, $m_Q (\gg \Lambda_{\text{QCD}})$, and the color-singlet nature of the bound states restrict the relevant dynamical degrees of freedom to be in a short-distance region and the asymptotic freedom of QCD designates expansions in a small coupling constant.

The purpose of this lecture is to provide a theoretical basis to study properties of the heavy $Q\bar{Q}$ system in perturbative QCD. In particular, we describe the nature of the force between Q and \bar{Q} and of their masses inside the bound states. Indeed, these ingredients determine the main dynamics inside the heavy quarkonium states. For pedagogical reasons, in this lecture we restrict our discussion to the leading-order contributions in the heavy mass limit $m_Q \rightarrow \infty$ and also in the leading logarithmic (LL) order of the perturbative series. With these tools, we provide a microscopic description of the interquark force and quark masses.

Some key aspects are as follows. First, higher-order terms of perturbative expansions play crucial roles to study properties of the heavy $Q\bar{Q}$ bound states quantitatively as well as qualitatively. In fact, their properties often turn out to be quite far from those of the Coulomb bound states such as positronium states. Secondly, it is important to separate systematically ultra-violet (UV) and infra-red (IR) energy scales involved. For this purpose it is essential to use a low-energy effective field theory (EFT) for a heavy $Q\bar{Q}$ system, such as potential-NRQCD (pNRQCD).

An interesting feature is that different theoretical frameworks and various concepts are mutually linked and converge towards a consistent picture. Namely, IR renormalons in the purely perturbative computation, OPE in an EFT, and extraction of UV contributions after log resummations, all point to a consistent result, which also agrees with results of lattice computations. At the same time we find an interrelation between the concepts of the running coupling constant, linear potential and quark self-energies (which resemble constituent quark masses) from a microscopic viewpoint, even though the validity range of the theory is restricted to a short-distance region $r < \Lambda_{\text{QCD}}^{-1}$. These subjects are covered in the main body of the lecture.

Let us sketch the outline of the lecture. (See also the table of contents in page 1.)

- Sec. 2:** After explaining the setup, we provide a microscopic picture of spontaneous breakdown of chiral symmetry and introduce the concept of constituent quark mass.
- Sec. 3:** To facilitate the reading for beginners, we explain the basic tools such as renormalization in the $\overline{\text{MS}}$ scheme, renormalization-group (RG) equation and running coupling constant.
- Sec. 4:** In order to study the interquark force, we define the static QCD potential from a Wilson loop and relate it to the energy of a heavy $Q\bar{Q}$ system.
- Sec. 5:** We explain the notion of IR renormalons as uncertainties characteristic to perturbative series.
- Sec. 6:** It is shown that the most dominant renormalon uncertainty cancels in a color-singlet heavy $Q\bar{Q}$ system, which leads to a dramatic improvement of convergence of perturbative series.
- Sec. 7:** We present a systematic method for a short-distance expansion of the UV contributions to the QCD potential and show that it predicts a “Coulomb+linear” potential in perturbative QCD.
- Sec. 8:** We provide a microscopic picture and interpretation of the heavy $Q\bar{Q}$ system, which can be obtained by the preceding analyses.
- Sec. 9:** We construct pNRQCD EFT from full QCD and explain the relation between an operator-product expansion (OPE) and renormalons. A solid theoretical framework to analyze the interquark force is provided.
- Sec. 10:** We list up references for each of Secs. 2–9 and for further applications, to assist the readers who want to learn the subjects more deeply or those who are interested in computations of various observables of heavy quarkonium states.

We collect technical details and necessary knowledge from related fields in appendices. To keep simplicity of explanations, in the main body of the lecture we do not quote related papers or describe how the relevant researches were carried out historically, apart from some monumental papers. The references are collected in the final section. Even there, we tend to refer to review-like recent papers, from which interested readers can trace original papers and details of researches at the frontiers.

Before starting the whole discussion, let us quote the current status of the static QCD potential. Fig. 1 shows the potential energy between two static color charges as a function of the distance r between the charges. The scales are measured in units of the QCD scale in the $\overline{\text{MS}}$ scheme at three-loop order, $\Lambda_{\overline{\text{MS}}}^{3\text{-loop}}$. The next-to-next-to-next-to-leading order (NNNLO) perturbative QCD prediction and lattice computations are compared. The three solid lines correspond to the perturbative predictions with different

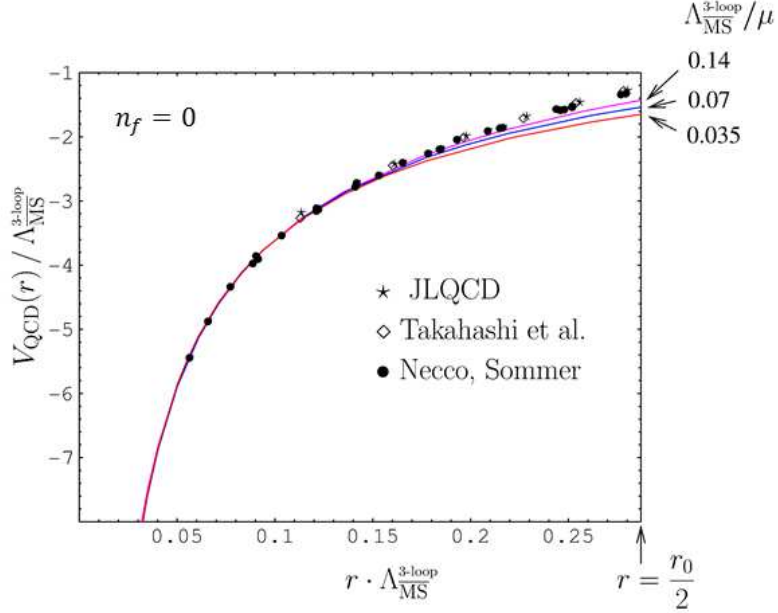


Figure 1: Static QCD potential as a function of the distance between the static charges r . Both axes are scaled by powers of $\Lambda_{\overline{\text{MS}}}^{3\text{-loop}}$. Solid lines represent NNNLO perturbative QCD predictions with different scale choices. Data points represent lattice computations by three different groups.

scale choices.[†] The data points represent lattice results by three different groups. The number of quark flavors n_f is set to zero in both computations. r_0 denotes the Sommer scale, which is interpreted as about 0.5 fm. Hence, the largest r in this figure is about 0.25 fm [$\approx (0.8 \text{ GeV})^{-1}$]. Since the relation between the lattice scale (r_0) and $\Lambda_{\overline{\text{MS}}}^{3\text{-loop}}$ is taken from other source, the only adjustable parameter in this comparison is an r -independent constant added to each potential, whose value is chosen such that all the potentials coincide at $r\Lambda_{\overline{\text{MS}}}^{3\text{-loop}} = 0.1$. We see a good agreement between the perturbative and lattice predictions in the displayed range.

2 QCD Lagrangian, Chiral Symmetry, Quark Masses

2.1 Setup

The chiral quark fields are defined as eigenstates of γ_5 as

$$\gamma_5 \psi_L(x) = -\psi_L(x), \quad \gamma_5 \psi_R(x) = +\psi_R(x), \quad (1)$$

where ψ_L and ψ_R represent the left-handed and right-handed quark fields, respectively. The QCD Lagrangian is given by

$$\begin{aligned} \mathcal{L}_{\text{QCD}} = & \sum_{q=u,d,s,c,b,t} \left[\overline{\psi}_L^{(q)} i \not{D} \psi_L^{(q)} + \overline{\psi}_R^{(q)} i \not{D} \psi_R^{(q)} - m_q \left(\overline{\psi}_L^{(q)} \psi_R^{(q)} + \overline{\psi}_R^{(q)} \psi_L^{(q)} \right) \right] \\ & - \frac{1}{4} G_{\mu\nu}^a G^{\mu\nu a}, \end{aligned} \quad (2)$$

[†] It is customary to vary the renormalization scale μ by a factor 2 or 1/2 in estimating uncertainties of perturbative QCD predictions.

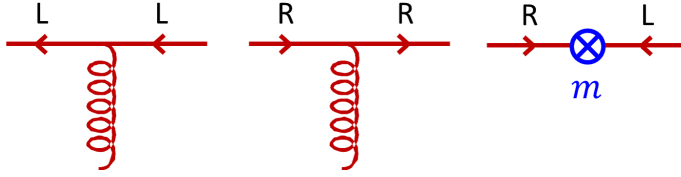


Figure 2: Chirality-conserving and chirality-violating vertices, which follow from eq. (4).

where the covariant derivative is given by $D_\mu = \partial_\mu - igA_\mu$.

Chiral transformation rotates ψ_L and ψ_R independently as

$$\psi_L \rightarrow e^{i\theta_L} \psi_L, \quad \psi_R \rightarrow e^{i\theta_R} \psi_R. \quad (3)$$

The quark part of the Lagrangian consists of invariant and non-invariant terms under this transformation:

$$\bar{\psi}(i\not{D} - m)\psi = \underbrace{\bar{\psi}_L i\not{D} \psi_L + \bar{\psi}_R i\not{D} \psi_R}_{\text{chiral inv.}} - m \underbrace{(\bar{\psi}_L \psi_R + \bar{\psi}_R \psi_L)}_{\text{chiral non-inv.}}, \quad (4)$$

where we omit the flavor indices. Chiral invariance is synonymous to chirality conservation, which means that a left-handed (right-handed) quark remains to be left-handed (right-handed) through interactions; see Fig. 2.

In QCD it is believed that, even if all the masses of quarks vanish ($m_q \rightarrow 0$), hadrons would still remain massive, and the order parameter of the chiral symmetry (chiral quark condensate) would remain non-zero:

$$\langle 0 | \bar{\psi}_L \psi_R + \bar{\psi}_R \psi_L | 0 \rangle \neq 0. \quad (5)$$

In fact, in Nature, the $\overline{\text{MS}}$ masses of the u and d quarks are much smaller than the proton and neutron masses:

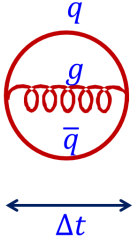
$$m_u \approx 2 \text{ MeV}, \quad m_d \approx 5 \text{ MeV} \ll m_p \approx m_n \approx 1 \text{ GeV}. \quad (6)$$

Conventionally this observation has led to the notion of the “constituent quark mass” of order 300 MeV, possessed by each quark inside a nucleon. It is considered as indicating spontaneous breakdown of chiral symmetry in the ideal limit $m_q \rightarrow 0$, and that chirality is not conserved by the QCD vacuum.

2.2 Picture of spontaneous chiral symmetry breakdown

Let us present a qualitative picture at a microscopic level of the spontaneous breakdown of chiral symmetry in the QCD vacuum.

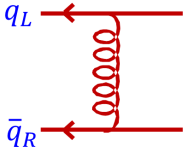
Suppose that initially the state is equal to the perturbative vacuum state, namely the ground state of the free field theory (the state without any quarks and gluons). As time



evolves, the QCD interaction generates quantum fluctuations. As indicated by the left diagram, a quark-antiquark pair and gluon can be created from the perturbative vacuum, for a short time interval determined by the uncertainty principle,

$$\Delta t \cdot \Delta E \sim 1. \quad (7)$$

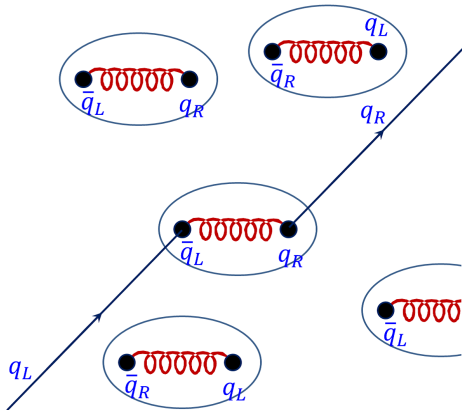
ΔE denotes the energy required to create the three particles. As ΔE becomes smaller, the lifetime of $q\bar{q}g$ becomes longer. ΔE is given by the sum of the energies of the individual particles, minus the binding energy E_{bin} . The largest binding energy is expected to be induced by an attractive force between the left-handed quark and right-handed antiquark* (\bar{q}_R) by exchange of gluons. Since the energy of each particle is not smaller than its rest energy (mass), the energy of the system is bounded from below as



$$\Delta E \geq 2m_q - E_{\text{bin}}. \quad (8)$$

E_{bin} is expected to be large, since the attractive force by QCD interaction is strong. If the quark masses are small, the binding energy may exceed $2m_q$. It is conjectured that this is the case for $q = u, d$, such that ΔE turns negative.

In the case $\Delta E > 0$, the lifetime of $q\bar{q}g$ becomes longer as ΔE decreases. If ΔE decreases further and turns negative, it becomes energetically more favorable (compared to the perturbative vacuum without any particles) to create quarks and gluons and lower the energy of the whole system by the large binding energy. Hence, $\bar{q}_L q_R$ and $\bar{q}_R q_L$ bound states are created everywhere, a large energy is emitted, and the total energy of the whole system gets lowered down. This is the condensation of $\bar{q}q$, by which essentially the space is covered with $\bar{q}q$ bound states, whose energies are lower than that of the perturbative vacuum. This state constitutes the true vacuum of QCD.



Since there are $\bar{q}_L q_R$ everywhere in the true vacuum, if a q_L propagates through this vacuum, it sometimes pair-annihilates with \bar{q}_L in a $\bar{q}_L q_R$ bound state. Then, q_R loses its partner and starts propagating in place of q_L . (See the left figure.) Thus, it looks as if q_L has turned into q_R while propagating through the vacuum.

Let us depict the same process in a Feynman diagrammatic manner. As can be seen in Fig. 3(a), the fundamental interaction always preserves chirality, in the limit $m_q \rightarrow 0$. Nevertheless, propagation of a quark in the vacuum looks as if chirality is non-conserving, if one does not see the structure of the vacuum; see Fig. 3(b).

* More precisely, it is an anti-particle of a right-handed quark, $(\overline{q_R})$. Nevertheless we use the short-hand terminology and notation, for brevity.

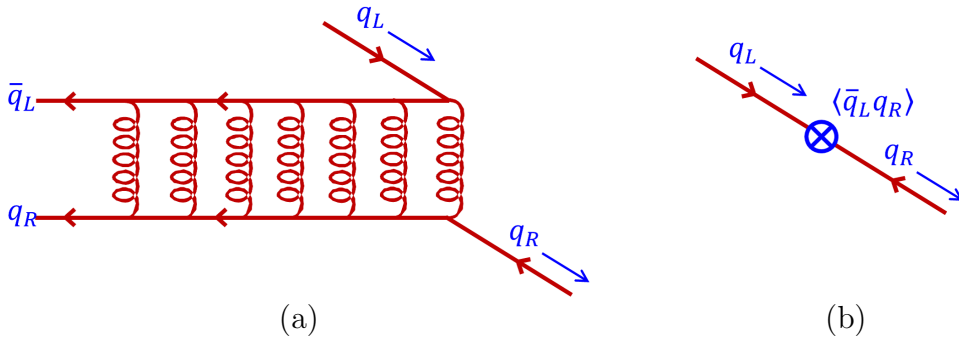


Figure 3: (a) Schematic picture of chirality transition when a quark propagates through the vacuum, depicted in a Feynman diagrammatic manner. (Time evolves from left to right.) The ladder-type multiple gluon exchanges symbolize a bound state of $\bar{q}_L q_R$. Note that chirality is preserved at the level of fundamental interaction. (b) Chirality violation by quark condensate in the vacuum with spontaneous symmetry breaking, when one does not see the structure of the vacuum.

To quantify the above picture, we need to perform a non-perturbative analysis, e.g., to use Nambu-Jona-Lasino model, Schwinger-Dyson equation, or lattice QCD simulation. Nevertheless, some aspects can be elucidated even within perturbative QCD, as we will see in the subsequent sections. It is not possible to describe spontaneous-symmetry-breaking phenomenon in perturbative QCD. It is, however, possible to access the “constituent quark mass picture,” which used to be considered also impossible. We will quantify to which extent this can be handled in perturbative QCD.

At this stage let us ask a paradoxical question. On the one hand, the constituent quark mass is known to be larger than the $\overline{\text{MS}}$ mass inside a nucleon. Hence, QCD interaction would increase the mass of a quark. On the other hand, just like the hydrogen atom, the mass of a heavy quarkonium is expected to be lighter than the sum of the masses of the individual heavy quarks, due to a negative binding energy. Hence, in this case, the masses of the quarks seem to be reduced by QCD interaction. The question is, whether QCD interaction increases or decreases the masses of quarks inside hadrons? It is one of the goals of this lecture that at the end the readers can answer to this question from a microscopic viewpoint.

3 $\overline{\text{MS}}$ scheme and Running Coupling Constant

In the following sections we perform analyses of logarithms in the perturbative prediction for the interquark force. They are based on the renormalization group (RG) equation, and we will prepare necessary theoretical basis in this section. Those who are familiar with this subject may as well skip this section.

3.1 Renormalization and $\overline{\text{MS}}$ scheme

Let us explain the renormalization procedure in perturbative QCD. In particular we explain the $\overline{\text{MS}}$ scheme, which is the most frequently used renormalization prescription in contemporary computations in perturbative QCD.

For simplicity we focus only on the gauge field, namely we ignore the quark and ghost fields in this subsection (which can be treated in a similar manner). The Lagrangian is given by

$$\mathcal{L}_A = -\frac{1}{4}G_{\mu\nu}^a G^{\mu\nu a}; \quad G_{\mu\nu}^a = \partial_\mu A_\nu^a - \partial_\nu A_\mu^a + g f^{abc} A_\mu^b A_\nu^c. \quad (9)$$

\mathcal{L}_A is expressed in terms of the bare field and bare coupling constant. We work with dimensional regularization and set the dimensions of the space-time as $D = 4 - 2\epsilon$ (one temporal and $(3-2\epsilon)$ spatial dimensions). Here, ϵ is treated as a general complex variable. In D dimensions, the (bare) gauge coupling constant is a dimensionful parameter. The gauge coupling and gauge field are rewritten in terms of the renormalized quantities as

$$g = \bar{\mu}^\epsilon Z_g g_R, \quad A_\mu = \sqrt{Z_A} A_\mu^R, \quad (10)$$

where $\bar{\mu}$ is a parameter with the dimension of mass, while the renormalization constants Z_i and renormalized coupling constant g_R are defined to be dimensionless; A_μ^R denotes the renormalized gauge field. If we choose $Z_i = Z_i(\epsilon, g_R)$ appropriately such that they diverge as $\epsilon \rightarrow 0$, perturbative series of all the physical quantities (S -matrix elements, cross sections, spectrum, etc.) can be made UV finite ('t Hooft).

In the first equation of (10), we separate the single parameter g of the theory into the parameters $\bar{\mu}$ and g_R (and Z_g). Since the number of parameters in the theory should not change, $\bar{\mu}$ (which will be rewritten by μ later) and $\alpha_s = \frac{g_R^2}{4\pi}$ are related if we fix the bare coupling. Therefore, we obtain the renormalized coupling constant as a function of the renormalization scale μ :

$$\alpha_s = \alpha_s(\mu). \quad (11)$$

Theoretical predictions are unchanged if α_s and μ are varied satisfying this relation.

In the $\overline{\text{MS}}$ scheme, we rewrite

$$\bar{\mu} = \frac{\mu}{\sqrt{4\pi}} e^{\gamma_E/2}, \quad (12)$$

where $\gamma_E = 0.5772 \dots$ denotes the Euler constant, and the renormalization constant is taken in the form

$$\begin{aligned} Z_g = 1 &+ \frac{\alpha_s(\mu)}{4\pi} \frac{Z_{11}}{\epsilon} + \left(\frac{\alpha_s(\mu)}{4\pi}\right)^2 \left(\frac{Z_{22}}{\epsilon^2} + \frac{Z_{21}}{\epsilon}\right) \\ &+ \left(\frac{\alpha_s(\mu)}{4\pi}\right)^3 \left(\frac{Z_{33}}{\epsilon^3} + \frac{Z_{32}}{\epsilon^2} + \frac{Z_{31}}{\epsilon}\right) + \dots \end{aligned} \quad (13)$$

We take Z_A also in the same form. Namely, only the poles of ϵ are included in Z_i , whereas order $\epsilon^0, \epsilon^1, \epsilon^2, \dots$ terms are not included.[†] In this way Z_i 's are defined uniquely and the renormalization prescription is fixed ($\overline{\text{MS}}$ scheme).

The reason why the $\overline{\text{MS}}$ scheme is used more often than other schemes is that empirically perturbative series for various physical quantities exhibit good convergence behaviors.

3.2 Renormalization group and running coupling constant

Let us consider an observable $A = A(\alpha_s(\mu); \mu/Q)$, which includes only one scale Q . We normalize A by powers of Q such that it becomes dimensionless. A typical example of A is the R -ratio in the case that quark masses are neglected; in this case $Q = \sqrt{s}$ represents the c.m. energy.

If we compute A in perturbative expansion, we obtain a polynomial of $\log(\mu/Q)$ in the form

$$A(\alpha_s(\mu); \mu/Q) = a_0 + a_1 \alpha_s(\mu) + \alpha_s(\mu)^2 \left[a_2^{(1)} \log\left(\frac{\mu}{Q}\right) + a_2^{(0)} \right] + \alpha_s(\mu)^3 \left[a_3^{(2)} \log^2\left(\frac{\mu}{Q}\right) + a_3^{(1)} \log\left(\frac{\mu}{Q}\right) + a_3^{(0)} \right] + \dots \quad (14)$$

Dependence on μ/Q of a single-scale observable emerges only through $\log(\mu/Q)$, due to the following reason. Since g is proportional to μ^ϵ ,[‡] at each order of perturbative expansion, μ/Q appears in the form $(\mu/Q)^\epsilon = 1 + \epsilon \log(\mu/Q) + \frac{1}{2}\epsilon^2 \log^2(\mu/Q) + \dots$. We expand in ϵ and send $\epsilon \rightarrow 0$ after subtracting poles in ϵ , hence we obtain powers of $\log(\mu/Q)$.

According to the previous subsection, physical quantities are independent of μ if we fix the bare coupling constant, or if $\alpha_s(\mu)$ is varied appropriately. This leads to the RG equation:

$$0 = \mu \frac{d}{d\mu} A(\alpha_s(\mu); \mu/Q) = \left[\mu \frac{\partial}{\partial \mu} + \mu \frac{d\alpha_s(\mu)}{d\mu} \frac{\partial}{\partial \alpha_s(\mu)} \right] A(\alpha_s(\mu); \mu/Q), \quad (15)$$

where we take into account the fact that μ dependence enters directly as well as indirectly through $\alpha_s(\mu)$. From the above equation, the beta function is defined by

$$\beta(\alpha_s(\mu)) = \mu \frac{d\alpha_s(\mu)}{d\mu}, \quad (16)$$

which is independent of the observable.

[†] Physical quantities can be made finite even if we include terms of order $\epsilon^0, \epsilon^1, \epsilon^2, \dots$ in Z_i . This corresponds to taking other renormalization prescription.

[‡] This is the only source of μ .

A formal solution to the RG equation (15) can be derived as follows. Let $t = \log(\mu/Q)$, then $\frac{\partial}{\partial t} = \mu \frac{\partial}{\partial \mu}$. Hence, the RG equation has a similar form to the Schrödinger equation in quantum mechanics:

$$\left(\frac{\partial}{\partial t} - \hat{H} \right) A(\alpha_s; t) = 0 \quad \text{with} \quad \hat{H} = -\beta(\alpha_s) \frac{\partial}{\partial \alpha_s}. \quad (17)$$

Its formal solution is given by

$$\begin{aligned} A(\alpha_s; t) &= e^{\hat{H}t} A(\alpha_s; t=0) = \sum_{n=0}^{\infty} \frac{t^n}{n!} \hat{H}^n A(\alpha_s; t=0) \\ &= \sum_{n=0}^{\infty} \frac{\log^n(\mu/Q)}{n!} \left[-\beta(\alpha_s) \frac{\partial}{\partial \alpha_s} \right]^n \left(a_0 + a_1 \alpha_s + a_2^{(0)} \alpha_s^2 + a_3^{(0)} \alpha_s^3 + \dots \right), \end{aligned} \quad (18)$$

where eq. (14) is used to rewrite $A(\alpha_s; t=0)$. This means that, if we know $\beta(\alpha_s)$ and the log-independent terms of $A(\alpha_s; \log(\mu/Q))$, all the log-dependent terms are determined by the RG equation.

The beta function can be determined from eqs. (15) and (16) using any observable A . By explicit perturbative computations, it is known to have a form

$$\beta(\alpha_s) = -b_0 \alpha_s^2 - b_1 \alpha_s^3 - b_2 \alpha_s^4 - \dots. \quad (19)$$

So far, the expansion coefficients have been computed up to b_3 .

Let us insert eq. (19) to eq. (18) and compute the first few terms.

- $n = 1$

$$-\beta(\alpha_s) \frac{\partial}{\partial \alpha_s} \alpha_s = -\beta(\alpha_s) = b_0 \alpha_s^2 + b_1 \alpha_s^3 + b_2 \alpha_s^4 + \dots, \quad (20)$$

- $n = 2$

$$\begin{aligned} \left[-\beta(\alpha_s) \frac{\partial}{\partial \alpha_s} \right]^2 \alpha_s &= (b_0 \alpha_s^2 + b_1 \alpha_s^3 + b_2 \alpha_s^4 + \dots) \frac{\partial}{\partial \alpha_s} [\text{RHS of eq. (20)}] \\ &= 2b_0^2 \alpha_s^3 + 5b_0 b_1 \alpha_s^4 + \dots, \end{aligned} \quad (21)$$

- $n = 3$

$$\left[-\beta(\alpha_s) \frac{\partial}{\partial \alpha_s} \right]^3 \alpha_s = 3! b_0^3 \alpha_s^4 + 26b_0^2 b_1 \alpha_s^5 + \dots, \quad (22)$$

⋮

⋮

Repeating the same procedure, and noting that differentiation by α_s reduces the power of α_s by one while $\beta(\alpha_s)$ raises the power by at least two, we find that the coefficients

of logarithms in eq. (14) are determined by the beta function and $a_1, a_i^{(0)}$'s to have the following form:

$$A(\alpha_s; \mu/Q) = a_0 + \sum_{n=0}^{\infty} \left\{ \underbrace{a_1 \alpha_s \left[b_0 \alpha_s \log\left(\frac{\mu}{Q}\right) \right]^n}_{\text{LL}} + \underbrace{C_n^{\text{NLL}} \alpha_s^2 \left[b_0 \alpha_s \log\left(\frac{\mu}{Q}\right) \right]^n}_{\text{NLL}} + \dots \right\}, \quad (23)$$

where C_n^{NLL} is given by a linear combination of $a_2^{(0)}/b_0$ and b_1/b_0 . The terms, which have n th power of $\log(\mu/Q)$ and $(n+1)$ th power of α_s , are called the leading logarithmic (LL) terms; the terms, which have one additional power of α_s compared to the LL terms, are called the next-to-leading logarithmic (NLL) terms, etc.

In the case that α_s is small but $b_0 \alpha_s \log(\mu/Q)$ is not small, it is necessary to resum the LL terms, since terms with higher n are not suppressed. It is expected that NLL terms and beyond are comparatively smaller, since α_s is small. It is possible to resum the LL terms if one knows b_0 and a_1 . Likewise, it is possible to resum the NLL terms if one knows b_1 and $a_2^{(0)}$ in addition, and so on. The necessity of resummation occurs when one wants to predict the observable in a wide range of Q , so that μ/Q varies substantially.

As we have seen, the leading (one-loop) coefficient of the beta function, b_0 , in

$$\mu \frac{d\alpha_s(\mu)}{d\mu} = -b_0 \alpha_s(\mu)^2 - b_1 \alpha_s(\mu)^3 - \dots \quad (24)$$

dictates the LL terms. For pedagogical reasons, in the following we mostly ignore b_1, b_2, \dots and constrain the argument to the LL case. Furthermore, we write

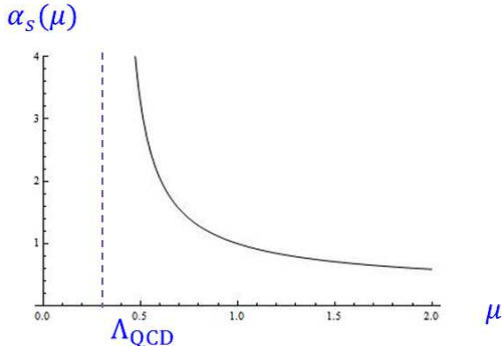
$$b_0 = \frac{\beta_0}{2\pi} \quad (25)$$

in the rest of this lecture.

The solution to the differential equation (24) in the case $b_1 = b_2 = \dots = 0$ and the replacement (25) defines the one-loop running coupling constant

$$\alpha_s(\mu) = \frac{2\pi}{\beta_0 \log(\mu/\Lambda_{\text{QCD}})}, \quad (26)$$

where Λ_{QCD} is a constant of integration. The inverse relation is given by



$$\Lambda_{\text{QCD}} = \mu \exp \left[-\frac{2\pi}{\beta_0 \alpha_s(\mu)} \right]. \quad (27)$$

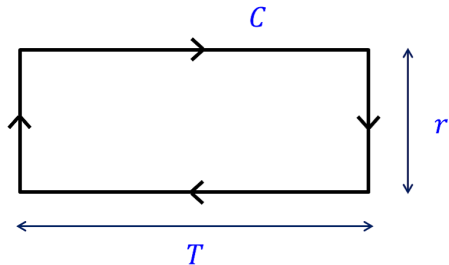
The running coupling constant $\alpha_s(\mu)$ is shown in the left figure. Λ_{QCD} is the scale where the coupling becomes large, $\alpha_s(\mu) \gtrsim \mathcal{O}(1)$, and the perturbation theory breaks down. By comparing to experimental values, it is known that roughly $\Lambda_{\text{QCD}} \sim 200\text{--}300$ MeV.

4 Interquark Force and QCD Potential

In this section we introduce the static QCD potential, which has long been analyzed to study the nature of the force between an infinitely heavy (static) quark-antiquark pair.

4.1 QCD potential from Wilson loop

Consider a Wilson loop



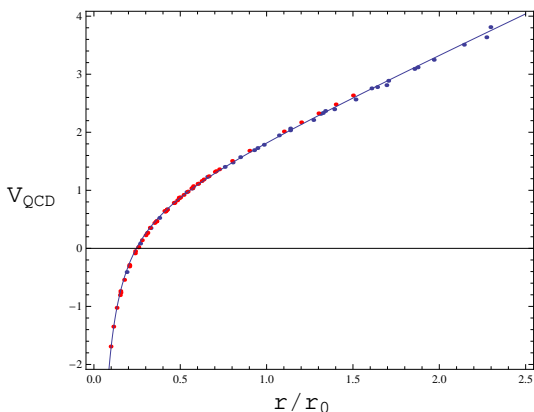
$$W[A_\mu] = \text{Tr} \left[\text{P exp} \left\{ ig \oint_C dx^\mu A_\mu(x) \right\} \right]. \quad (28)$$

Here, the integral contour C is taken to be rectangular, of spatial extent r and time extent T ; see the left figure. P stands for the path-ordered product along the contour C . (Note that $A_\mu(x)$ at different x do not generally commute.) We define the static

QCD potential $V_{\text{QCD}}(r)$, from the expectation value of the Wilson loop in the large T limit, by

$$\begin{aligned} \langle W[A_\mu] \rangle &= \int \mathcal{D}A_\mu \mathcal{D}\psi_q \mathcal{D}\bar{\psi}_q W[A_\mu] \exp \left(i \int d^4x \mathcal{L}_{\text{QCD}} \right) \\ &\approx \text{const.} \times \exp [-iT V_{\text{QCD}}(r)] \quad \text{as } T \rightarrow \infty. \end{aligned} \quad (29)$$

As will be explained in the next subsection, $V_{\text{QCD}}(r)$ represents the energy between heavy quarks (static color charges).



Known from numerical computations by lattice simulations, $V_{\text{QCD}}(r)$ can be fitted well by a “Coulomb+linear” form.*

$$V_{\text{QCD}}(r) \approx -\frac{a}{r} + Kr + \text{const.} \quad (30)$$

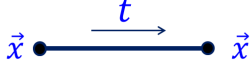
We show in the left figure lattice computations of $V_{\text{QCD}}(r)$ by two different groups and a fit of these numerical data by the above “Coulomb+linear” form. In general, lattice simulations can compute $V_{\text{QCD}}(r)$ accurately at large r , whereas perturbative QCD can predict $V_{\text{QCD}}(r)$ more accurately at small r .

There has been a kind of folklore that in eq. (30) the perturbative prediction gives the Coulomb part $-a/r$, while non-perturbative contribution gives the linear part Kr , and both contributions add up.[†] We will show that at least at short distances, $r \lesssim 0.5$ fm, this statement is incorrect, in that the linear part is included in perturbative prediction.

* It has also been known that phenomenological potentials, which reproduce the measured bottomonium and charmonium spectra, have shapes close to $V_{\text{QCD}}(r)$ computed by lattice simulations.

[†] There is an indication in this direction. In lattice simulations with gauge fixing in maximally

4.2 Energy of a static quark pair



In order to clarify the meaning of the static QCD potential, we rewrite the Wilson line by path integral. The Wilson line in the time direction (see left) can be written as[‡]

$$\text{P exp} \left[ig \int_0^T dt A_0(t, \vec{x}) \right] \delta^3(\vec{x} - \vec{y}) = \int \mathcal{D}\psi \mathcal{D}\psi^\dagger \psi(T, \vec{x}) \psi^\dagger(0, \vec{y}) \exp \left[i \int d^4x \mathcal{L}_{\text{HQET}} \right], \quad (T \geq 0) \quad (31)$$

where $\psi(x)$ is a complex scalar field,[§] which belongs to the N representation of $SU(N)$ gauge group. ($N = 3$ for QCD.) $\mathcal{L}_{\text{HQET}}$ denotes the Lagrangian of the Heavy Quark Effective Theory (HQET), given by

$$\mathcal{L}_{\text{HQET}} = \psi(x)^\dagger i D_t \psi(x), \quad D_t = \partial_t - ig A_0(x). \quad (32)$$

The Feynman rules of HQET are shown in Fig. 4 below.

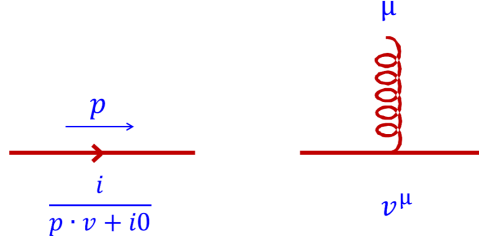


Figure 4: Feynman rules of HQET. The left diagram represents the heavy quark propagator, and the right diagram represents the gluon vertex. $v^\mu = (1, \vec{0})$ denotes the unit vector in the time direction.

The equality (31) can be shown in the following manner. Since $\mathcal{L}_{\text{HQET}}$ is bilinear in ψ , the path integral on the right-hand side can be performed to yield

$$[\text{RHS of eq. (31)}] = D_t^{-1}(T, \vec{x}; 0, \vec{y}), \quad (33)$$

which means that it is the kernel of the covariant derivative D_t :

$$\left[\partial_t - ig A_0(T, \vec{x}) \right] [\text{RHS of eq. (31)}] = \delta(T) \delta^3(\vec{x} - \vec{y}). \quad (34)$$

abelian gauge, it is known that $V_{\text{QCD}}(r)$ can be approximated well by the sum of the contribution from ‘abelian gluons,’ which gives a Coulomb-like potential, and the contribution from monopoles, which gives rise to a linear potential. This feature seems to be valid down to fairly short distances.

[‡] The delta function on the left-hand side follows from the usual equal-time commutation relation of $\psi(t, \vec{x})$ and $\psi^\dagger(t, \vec{y})$.

[§] Since we deal only with zero- or one-particle states, it does not matter whether $\psi(x)$ is a boson or fermion. The point here is that we do not consider the spin degrees of freedom of the color charge.

On the other hand, at $T > 0$, we find

$$\begin{aligned} \left[\partial_t - igA_0(T, \vec{x}) \right] [\text{LHS of eq. (31)}] &= \left[igA_0(T, \vec{x}) - igA_0(T, \vec{x}) \right] [\text{LHS of eq. (31)}] \\ &= 0 \end{aligned} \quad (35)$$

by differentiation. Furthermore, if we take the limit $T \rightarrow 0$, we find

$$[\text{LHS, RHS of eq. (31)}] \rightarrow \delta^3(\vec{x} - \vec{y}). \quad (36)$$

Thus, both sides satisfy the same first-order differential equation with the same initial condition for $T \geq 0$.

Using the above relation, we can express the Wilson loop (28) as a path integral:

$$\begin{aligned} &W[A_\mu] \delta^3(\vec{x} - \vec{x}') \delta^3(\vec{y} - \vec{y}') \\ &= \int \mathcal{D}\psi \mathcal{D}\psi^\dagger \mathcal{D}\chi \mathcal{D}\chi^\dagger \exp \left[i \int d^4x (\psi^\dagger iD_t \psi + \chi^\dagger iD_t \chi) \right] \\ &\quad \times \underbrace{[\psi^\dagger(0, \vec{x}) \phi(\vec{x}, \vec{y}; 0) \chi(0, \vec{y})]}_{(i)} \underbrace{[\psi(T, \vec{x}') \phi^\dagger(\vec{x}', \vec{y}'; T) \chi^\dagger(T, \vec{y}')] }_{(ii)}, \end{aligned} \quad (37)$$

where $\psi(x)$ and $\chi(x)$ are both complex scalar fields in the N representation, and

$$\phi(\vec{x}, \vec{y}; t) = \text{P exp} \left[ig \int_{\vec{y}}^{\vec{x}} d\vec{x} \cdot \vec{A}(t, \vec{x}) \right] \quad (38)$$

denotes the color string spanned between \vec{x} and \vec{y} . Here, $\chi(x)$ represents the field, which *creates* the anti-color charge and belongs to the N representation (rather than \bar{N} representation). Namely, we adopt the definition, which corresponds to the anti-particle component of the Dirac field (i.e., $\chi \sim d^\dagger$ of $b_{\vec{p},s} e^{-i\vec{p}\cdot\vec{x}} + d_{\vec{p},-s}^\dagger e^{i\vec{p}\cdot\vec{x}}$). Eq. (37) is depicted in Fig. 5 below.

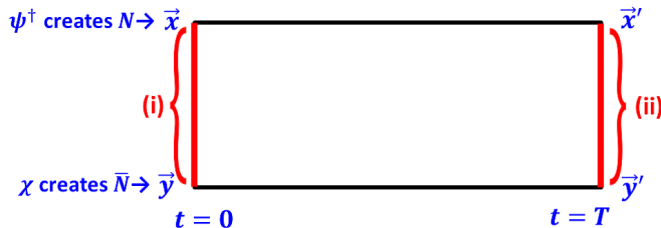


Figure 5: Correspondence between eq. (37) and the Wilson loop. Only the configuration $\vec{x} = \vec{x}'$ and $\vec{y} = \vec{y}'$ survives, since ψ and χ cannot propagate in the spatial direction.

We compute $V_{\text{QCD}}(r)$ from $\langle W[A_\mu] \rangle$ as given by eq. (29). Substituting the expression (37) [after dividing by $\delta^3(\vec{x} - \vec{x}') \delta^3(\vec{y} - \vec{y}')$], the Lagrangian of eq. (29) is replaced as

$$\mathcal{L}_{\text{QCD}} \rightarrow \mathcal{L}_{\text{QCD}} + \psi^\dagger iD_t \psi + \chi^\dagger iD_t \chi, \quad (39)$$

and there are insertions of the color source operators (i) and (ii). Starting from this expression we can compute the Wilson loop [and therefore $V_{\text{QCD}}(r)$] in perturbative QCD, using the Feynman rules in Fig. 4 in combination with those of QCD. The leading contribution to $V_{\text{QCD}}(r)$ is given by the diagram with one-gluon exchange between the two color charges at \vec{x} and \vec{y} , which simply gives a Coulomb potential.

Equivalently, we can express $\langle W[A_\mu] \rangle$ in canonical formulation. Let[¶]

$$|\alpha\rangle = \psi^\dagger(\vec{x}) \phi(\vec{x}, \vec{y}; 0) \chi(\vec{y}) |0\rangle, \quad (40)$$

$$|\beta\rangle = \psi^\dagger(\vec{x}') \phi(\vec{x}', \vec{y}'; T) \chi(\vec{y}') |0\rangle, \quad (41)$$

$$H = \int d^3\vec{x} (\mathcal{H}_{\text{QCD}} + ig \psi^\dagger A_0 \psi + ig \chi^\dagger A_0 \chi), \quad (42)$$

then we can express

$$\begin{aligned} \langle W[A_\mu] \rangle &= \frac{\langle \beta | e^{-iHT} | \alpha \rangle}{\delta^3(\vec{x} - \vec{x}') \delta^3(\vec{y} - \vec{y}')} \\ &\approx \text{const.} \times \exp[-iT V_{\text{QCD}}(r)] \quad \text{as } T \rightarrow \infty. \end{aligned} \quad (43)$$

This shows that $V_{\text{QCD}}(r)$ is the lowest energy eigenvalue of the energy eigenstates of H , which have overlaps with $|\alpha\rangle$ and $|\beta\rangle$. Indeed, by inserting completeness relation in terms of the eigenstates of H , we find

$$\begin{aligned} \langle \beta | e^{-iHT} | \alpha \rangle &= \sum_n \langle \beta | n \rangle \langle n | \alpha \rangle e^{-iE_n T} \\ &\longrightarrow \langle \beta | n_0 \rangle \langle n_0 | \alpha \rangle e^{-iE_{n_0} T} \quad \text{as } T \rightarrow \infty, \end{aligned} \quad (44)$$

where the lowest energy state $|n_0\rangle$ is selected by $+i0$ prescription, as usual.

One way to see that the Lagrangian (39) [or the Hamiltonian (42)] corresponds to inclusion of infinitely heavy colored particles may be as follows. The Lagrangian of the non-relativistic Schrödinger equation in quantum mechanics is given by

$$\mathcal{L}_{\text{QM}} = \psi^\dagger \left(iD_t - \frac{\vec{D}^2}{2m} \right) \psi. \quad (45)$$

If we send $m \rightarrow \infty$, it reduces to $\mathcal{L}_{\text{HQET}}$.

Thus, $V_{\text{QCD}}(r)$ can be interpreted as the energy between infinitely heavy (static) color charges, which are separated by distance $r = |\vec{x} - \vec{y}|$ and in a color-singlet state (since $|\alpha\rangle, |\beta\rangle$ are color singlet). The force between the static charges is obtained by differentiating $V_{\text{QCD}}(r)$:

$$F(r) = -\frac{d}{dr} V_{\text{QCD}}(r). \quad (46)$$

[¶] Since the HQET Lagrangian is first-order in time derivative, the Hamiltonian is given by dropping the kinetic term of the Lagrangian, similarly to the Dirac theory. (It can be derived from the path integral in holomorphic representation.)

5 Renormalons in QCD Potential

In this section we explain renormalons in the perturbative prediction of $V_{\text{QCD}}(r)$, which cause large theoretical uncertainties.

5.1 Theoretical background: asymptotic series

First we explain the notion of asymptotic series. As an example, we consider a one-dimensional integral

$$F(\lambda) = \int_{-\infty}^{\infty} dx e^{-\frac{1}{2}x^2 - \frac{\lambda}{4}x^4}, \quad (47)$$

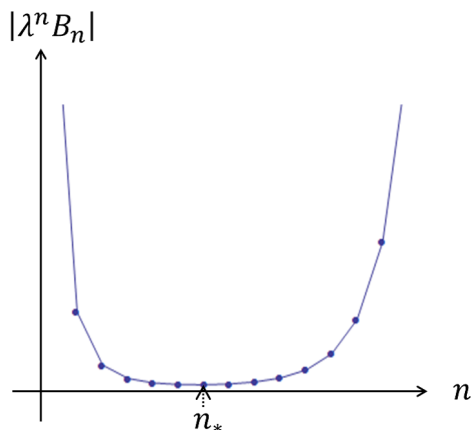
which is a toy model imitating the partition function of the $\lambda\phi^4$ theory. This integral has the following properties:

- The integral is well defined for $\text{Re } \lambda \geq 0$.
- The integral is divergent for $\text{Re } \lambda < 0$.
- $\lambda = 0$ is an essential singularity.

As a result, the convergence radius of the series expansion of F in λ is zero.* Namely, the series expansion does not converge for whatever small value of $|\lambda|$. In fact, the perturbative series can be computed as

$$F(\lambda) = \int_{-\infty}^{\infty} dx e^{-\frac{1}{2}x^2} \sum_{n=0}^{\infty} \frac{\left(-\frac{1}{4}\lambda x^4\right)^n}{n!} = \sum_{n=0}^{\infty} \lambda^n B_n, \quad (48)$$

$$B_n = \frac{\sqrt{2}(-1)^n}{n!} \Gamma\left(2n + \frac{1}{2}\right). \quad (49)$$



B_n grows rapidly for large n . Hence, for $|\lambda| \ll 1$, the series first converges apparently but starts diverging from some $n = n_*$; see the left figure,

Let us define the difference between the true value $F(\lambda)$ and the sum of a truncated series by

$$\delta F_N \equiv \left| F(\lambda) - \sum_{n=0}^N \lambda^n B_n \right| \quad (50)$$

for $\text{Re } \lambda \geq 0$ [such that $F(\lambda)$ is well defined]. It can be shown that $\delta F_N \sim \mathcal{O}(|\lambda^N B_N|)$. Namely,

* $F(\lambda)$ can be expressed analytically using the Bessel function, and its analytic properties can be studied in full detail.

for $N \lesssim n_*$, the truncated series approaches the true value as we include more terms. The best approximation is obtained if we truncate at $N \approx n_*$, where $\delta F_N \sim |\lambda^{n_*} B_{n_*}|$.

It is conjectured that in QCD $\alpha_s = 0$ is also an essential singularity. Therefore, at best, perturbative expansions in α_s would be asymptotic series. Explicit computations have shown that the perturbative expansion of $V_{\text{QCD}}(r)$ receives large radiative corrections even at low orders of expansion, which results in a theoretical uncertainty, $\delta V_{\text{QCD}}(r) \sim \Lambda_{\text{QCD}} \sim 200\text{--}300$ MeV. See Fig. 6. This feature can be understood qualitatively in terms of the renormalons.

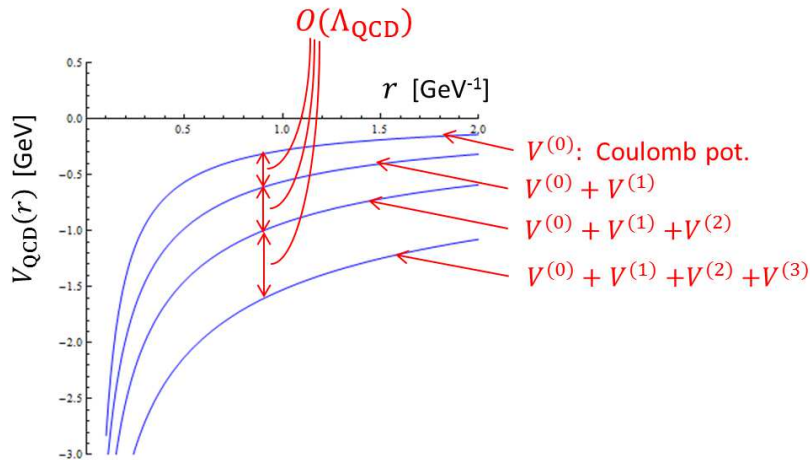


Figure 6: Truncated perturbative series of $V_{\text{QCD}}(r)$ up to the first four terms. At each order the potential receives a large correction, which is an almost negative r -independent shift of order Λ_{QCD} .

5.2 Renormalons in $V_{\text{QCD}}(r)$: some details

According to the argument in Sec. 3.2, the perturbative expansion of $V_{\text{QCD}}(r)$ takes a form:

$$V_{\text{QCD}}(r) = -\frac{C_F \alpha_s}{r} \left[1 + \frac{\alpha_s}{4\pi} \left\{ \beta_0 \log(\mu^2 r^2) + a_1 \right\} + \left(\frac{\alpha_s}{4\pi} \right)^2 \left\{ \beta_0^2 \log^2(\mu^2 r^2) + \dots \right\} + \dots \right], \quad (51)$$

where the Casimir operator of the fundamental representation is defined as $T_F^a T_F^a = C_F \mathbf{1}$, and $C_F = 4/3$ in QCD; β_0 is the coefficient of the one-loop beta function defined by

$$\mu \frac{d\alpha_s}{d\mu} = -\frac{\beta_0}{2\pi} \alpha_s^2 - \dots \quad (52)$$

Let us define a potential with LL resummation formally as

$$V_{\beta_0}(r) = - \int \frac{d^3 \vec{q}}{(2\pi)^3} e^{i\vec{q}\cdot\vec{r}} C_F \frac{4\pi \alpha_{1L}(q)}{q^2} \quad ; \quad q \equiv |\vec{q}|, \quad (53)$$

where

$$\alpha_{1\text{L}}(q) = \frac{2\pi}{\beta_0 \log(q/\Lambda_{\text{QCD}})} = \frac{\alpha_s(\mu)}{1 + \frac{\beta_0 \alpha_s(\mu)}{2\pi} \log\left(\frac{q}{\mu}\right)} \quad (54)$$

denotes the one-loop running coupling constant. In the second equality we substituted the relation (27). Use of $\alpha_{1\text{L}}(q)$ corresponds to resumming LLs in momentum space, since the expansion of $\alpha_{1\text{L}}(q)$ in $\alpha_s(\mu)$ gives a geometric series $\sum_n \left[\frac{\beta_0 \alpha_s(\mu)}{2\pi} \log\left(\frac{\mu}{q}\right) \right]^n$.

The integral in eq. (53) is ill defined, since $\alpha_{1\text{L}}(q)$ has a pole at $q = \Lambda_{\text{QCD}}$. Nevertheless, if we expand the integrand in $\alpha_s(\mu)$, the integral of each term is well defined. Thus, we obtain a perturbative series as

$$\begin{aligned} V_{\beta_0}(r) &= -C_F 4\pi \alpha_s(\mu) \sum_{n=0}^{\infty} \int \frac{d^3 \vec{q}}{(2\pi)^3} \frac{e^{i\vec{q}\cdot\vec{r}}}{q^2} \left[\frac{\beta_0 \alpha_s(\mu)}{4\pi} \log\left(\frac{\mu^2}{q^2}\right) \right]^n \\ &= -C_F 4\pi \alpha_s(\mu) \sum_{n=0}^{\infty} \left[\frac{\beta_0 \alpha_s(\mu)}{4\pi} \right]^n f_n(r, \mu) n!. \end{aligned} \quad (55)$$

Although each $f_n(r; \mu)$ is well defined, the perturbative expansion is an asymptotic series. This leads to an $\mathcal{O}(\Lambda_{\text{QCD}})$ uncertainty.

To clarify this statement, we define a generating function:[†]

$$F(r, \mu; u) \equiv \int \frac{d^3 \vec{q}}{(2\pi)^3} \frac{e^{i\vec{q}\cdot\vec{r}}}{q^2} \left(\frac{\mu^2}{q^2} \right)^u = \sum_n f_n(r, \mu) u^n \quad (57)$$

$$= \frac{1}{4\pi^{3/2} r} \left(\frac{\mu r}{2} \right)^{2u} \frac{\Gamma(\frac{1}{2} - u)}{\Gamma(1 + u)}. \quad (58)$$

This is called the Borel transform of $V_{\beta_0}(r)$. The same $f_n(r; \mu)$ as in eq. (55) appears, since $(\mu^2/q^2)^u = e^{u \log(\mu^2/q^2)} = \sum_n \frac{u^n}{n!} \log^n\left(\frac{\mu}{q}\right)$. The convergence of the series is accelerated by $1/n!$ compared to $V_{\beta_0}(r)$. As a result, it has a finite radius of convergence around $u = 0$.

The behavior of $f_n(r, \mu)$ at $n \gg 1$ can be determined from the analyticity of F in the complex u -plane (shown in Fig. 7). In fact, the large- n behavior of $f_n(r, \mu)$ determines the domain of convergence of the series expansion (57) at $u = 0$, while the pole of

[†] To derive the last expression, we rewrite

$$\left(\frac{1}{q^2} \right)^{u+1} = \frac{1}{\Gamma(1+u)} \int_0^\infty d\alpha \alpha^u e^{-\alpha q^2}, \quad (56)$$

then integrals over \vec{q} reduce to Gaussian integrals, which can be evaluated easily. The remaining integral over α can be expressed in terms of the Γ function.

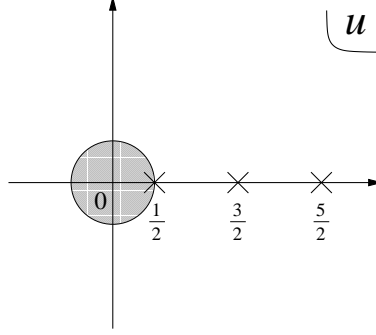


Figure 7: Analyticity of the generating function $F(r, \mu; u)$ shown in the complex u -plane. Poles are located at $u = \frac{1}{2}, \frac{3}{2}, \frac{5}{2}, \dots$. Also the domain of convergence of the series expansion at $u = 0$ is shown.

(58) closest to $u = 0$ determines the convergence radius. The closest pole is located at $u = 1/2$, included in $\Gamma(\frac{1}{2} - u)$. It follows that

$$f_n(r, \mu) \sim \frac{\mu}{2\pi^2} \times 2^n \quad \text{for } n \gg 1. \quad (59)$$

This is extracted from the contribution of the pole at $u = 1/2$.[‡]

$$F \sim \frac{1}{4\pi^{3/2} r} \left(\frac{\mu r}{2}\right)^1 \frac{1}{\frac{1}{2} - u} \frac{1}{\sqrt{\pi}/2} = \frac{\mu}{2\pi^2} \frac{1}{1 - 2u} = \sum_{n=0}^{\infty} \frac{\mu}{2\pi^2} \times 2^n u^n. \quad (60)$$

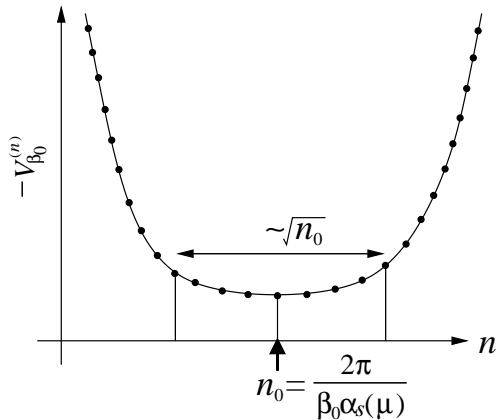
Hence, asymptotically, the n -th term of $V_{\beta_0}(r)$ is given by

$$\begin{aligned} V_{\beta_0}^{(n)} &\sim -C_F 4\pi\alpha_s \times \frac{\mu}{2\pi^2} \left(\frac{\beta_0\alpha_s}{2\pi}\right)^n \times n! \\ &= \text{const.} \times a^n n! \quad \text{with } a = \frac{\beta_0\alpha_s}{2\pi}. \end{aligned} \quad (61)$$

Note that it is independent of r . The r -dependence is canceled when we evaluate the residue of F at $u = 1/2$ in eq. (60). This means that, although each term $V_{\beta_0}^{(n)}(r)$ of the potential is a function of r , its dominant part for $n \gg 1$ is only a constant potential; see Fig. 6.

[‡] If we subtract the pole at $u = 1/2$ and consider $\sum_n \left[f_n(r; \mu) - \frac{\mu}{2\pi^2} 2^n \right] u^n = F - (\text{pole at } u = 1/2)$, the convergence radius enlarges to $3/2$. Namely, $|f_n - \frac{\mu}{2\pi^2} 2^n|$ at $n \gg 1$ decreases more rapidly than $|f_n|$. This means that the leading behavior of f_n at $n \gg 1$ is given by $\frac{\mu}{2\pi^2} 2^n$ [eq. (59)].

The behavior of $-V_{\beta_0}^{(n)}$ for a small α_s is shown schematically in the figure below.



As we raise n , first the term decreases due to powers of α_s ; for large n the term increases due to the factorial $n!$. Around $n \approx n_0$, the term becomes smallest. The size of the term scarcely changes within the range $n \in (n_0 - \sqrt{n_0}, n_0 + \sqrt{n_0})$.

We may find n_0 , which minimizes $-V_{\beta_0}^{(n)}$, as follows. The terms are almost identical in the neighborhood of n_0 , hence, $a^{n_0-1}(n_0-1)! \approx a^{n_0}n_0!$, which means

$$n_0 \approx \frac{1}{a} = \frac{2\pi}{\beta_0 \alpha_s(\mu)}. \quad (62)$$

It follows that

$$a^{n_0}n_0! \approx a^{1/a} \times \sqrt{\frac{2\pi}{a}} \left(\frac{1}{a}\right)^{1/a} e^{-1/a} = \sqrt{\frac{2\pi}{a}} e^{-1/a} \quad (63)$$

We may consider an uncertainty of this asymptotic series as the sum of the terms within the range $n_0 - \sqrt{n_0} < n < n_0 + \sqrt{n_0}$, since we are not certain where to truncate the series within this range:

$$\delta V_{\beta_0}(r) \sim \sum_{n=n_0-\sqrt{n_0}}^{n_0+\sqrt{n_0}} |V_{\beta_0}^{(n)}| \sim \Lambda_{\text{QCD}}. \quad (64)$$

The μ -dependence vanishes in this sum, and this leads to the claimed uncertainty.

The word “renormalon” denotes a pole (or more generally a singularity) in the complex u -plane (Borel plane), which dictates the large- n behavior with factorial growth of a perturbative expansion. The above estimate based on a renormalon reproduces well the qualitative feature of the known first four terms of the perturbative expansion of $V_{\text{QCD}}(r)$ shown in Fig. 6 (which does not use the LL approximation); see also Fig. 11 in Sec. 6.3 below. In comparison, the level spacings in the measured spectra of the bottomonium ($b\bar{b}$) and charmonium ($c\bar{c}$) states are not larger than order Λ_{QCD} . As a result, if the perturbative prediction for $V_{\text{QCD}}(r)$ is naively used to predict these spectra, predictability turns out to be very poor. This corresponds to the status before around 1998.

Before ending this section, we comment on the indication of renormalons. In the above argument, we start from an ill-defined integral and obtain renormalons and asymptotic series. One may wonder what is meant by a prediction by an asymptotic series when the original integral is ill-defined. We note that it is not the ill-defined nature of the integral that directly leads to the renormalons. In fact, one can construct examples, in which (1) the integral is well-defined and renormalons exist, and (2) the integral is ill-defined and there is no renormalon. The former case is realized, for instance, when

the two-loop coefficient β_1 of the beta function is included and has an opposite sign to the one-loop coefficient β_0 , so that the running coupling constant becomes large in the region $q \lesssim \Lambda_{\text{QCD}}$ but is still well defined down to $q = 0$.[§] The latter example is realized, when we constrain the integral region to $q > q_0$, where $0 < q_0 < \Lambda_{\text{QCD}}$. Considering these examples, it would be adequate to interpret in the following way: Renormalons signal that an effective expansion parameter becomes large at scale $q \lesssim \Lambda_{\text{QCD}}$ and validity of the perturbative expansion is breaking down in this part of the integral region. Later in this lecture, we will remedy this problem by eliminating contributions from the region $q \lesssim \Lambda_{\text{QCD}}$. It is important to investigate and identify which part of the perturbative prediction is free from ambiguities in the IR region, and in this context analysis of renormalons is useful.

6 Cancellation of Renormalons in Total Energy

We show that the uncertainty $\delta V_{\text{QCD}}(r) \sim \Lambda_{\text{QCD}}$ is canceled by the similar uncertainty included in the quark pole mass, for a system of a color-singlet heavy quark-antiquark pair. This leads to a higher predictive power of perturbative QCD for the energy of this system.

6.1 Quark pole mass and total energy of $Q\bar{Q}$ system

Define the total energy of a heavy $Q\bar{Q}$ system as

$$E_{\text{tot}}(r) \equiv 2m_{\text{pole}} + V_{\text{QCD}}(r), \quad (65)$$

where m_{pole} denotes the pole mass of the heavy quark. This constitutes the major part of the energy of the $Q\bar{Q}$ system, in the limit where the masses of the quarks are heavy. If m_{pole} is expressed in terms of the $\overline{\text{MS}}$ mass $m_{\overline{\text{MS}}}(\mu)$, the renormalon at $u = 1/2$ contained in $V_{\text{QCD}}(r)$ is canceled by the one contained in m_{pole} . Here, the two representative quark masses used in perturbative QCD have the following meanings:

Pole mass: the energy of a quark at rest, which is equivalent to the pole position of the quark propagator. All the contributions to the quark self-energy are included.

$\overline{\text{MS}}$ mass: a parameter in the Lagrangian $\sim -m_q \bar{\psi}_q \psi_q$, renormalized in the $\overline{\text{MS}}$ scheme (i.e., only UV divergence is subtracted). Only UV part of the quark self-energy is included.

These are depicted schematically in Fig. 8.

The notion of the quark pole mass contradicts the quark confinement picture. In fact, if the energy of a single quark, which has a color charge, is computed non-perturbatively, it is expected to be infinite. It is almost equivalent to the statement that, to separate a quark and an antiquark, one needs an energy proportional to the distance between

[§] In this case the renormalons are not poles but branch points in the Borel plane.



Figure 8: Since a quark has a color charge, gluons with arbitrarily wavelength λ_g can couple to the quark and contribute to the quark self-energy. m_{pole} , being the energy of a quark at rest, includes all the contributions from $0 < \lambda_g < \infty$. On the other hand, $m_{\overline{\text{MS}}}(\mu)$ is defined such that it includes only contributions from short wavelength $0 < \lambda_g \lesssim \mu^{-1}$.

the two particles (provided that the string breaking does not occur), so that to separate them infinitely apart, one needs an infinite energy.

In perturbative QCD, the pole mass can be computed to be finite, order by order in perturbative expansion. Nevertheless, it is expected to contain at least $\mathcal{O}(\Lambda_{\text{QCD}})$ uncertainty. To illustrate this, let us compare measurements of the masses of the W boson and top quark, respectively. As shown in Fig. 9(a), the W boson mass can be

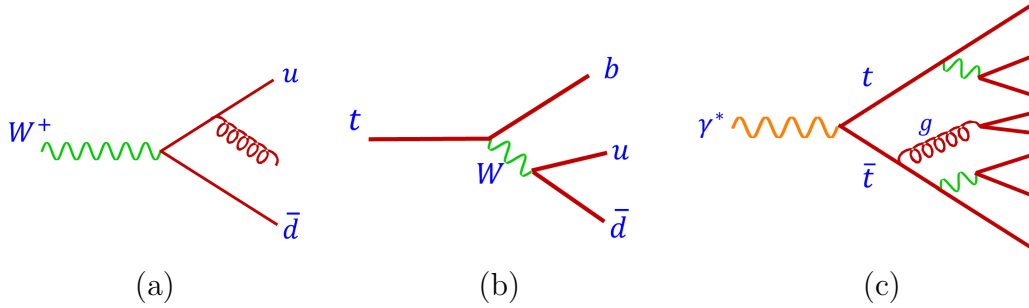


Figure 9: Relevant processes for measurements of the masses of the W boson and top quark from their hadronic decays. In (a), (b) and (c), the initial states are color-singlet, color-triplet and color-singlet, respectively. Unlike W boson, the momentum of top quark cannot be reconstructed unambiguously from the final state hadrons in experiments.

measured from the invariant mass of all the hadrons in its hadronic decay. The invariant mass coincides with the W mass, event by event (if we ignore the decay width of W and measurement errors). On the other hand, if we measure the invariant mass of all the hadrons, which come from the top quark in its hadronic decay, it does not coincide with the top quark mass. The top quark has a color, while hadrons in the final state are color singlet. Hence, top quark momentum and the sum of the hadron momenta do not coincide. See Fig. 9(b). If we consider pair creation of $t\bar{t}$ from a color singlet state, the total momenta of all the final state hadrons coincide with the sum of the t and \bar{t} momenta. However, it is non-trivial to separate the hadron momenta into t and \bar{t} sides. There should be uncertainty of at least order m_π in this assignment, event by event. See Fig. 9(c). Thus, the notion of the quark pole mass would be ambiguous beyond $\mathcal{O}(\Lambda_{\text{QCD}})$

accuracy, even if we consider a realistic situation to extract a quark pole mass from a physical process by comparison to perturbative QCD prediction, due to the presence of string breaking and color neutralization.

The expression of the quark pole mass in terms of the $\overline{\text{MS}}$ mass is given in perturbative series as

$$m_{\text{pole}} = m_{\overline{\text{MS}}}(\mu) \left[1 + \alpha_s(\mu) \left\{ d_{11} \log\left(\frac{\mu}{m_{\overline{\text{MS}}}}\right) + d_{10} \right\} + \alpha_s(\mu)^2 \left\{ d_{22} \log^2\left(\frac{\mu}{m_{\overline{\text{MS}}}}\right) + d_{21} \log\left(\frac{\mu}{m_{\overline{\text{MS}}}}\right) + d_{20} \right\} + \dots \right]. \quad (66)$$

We present the result for an estimate of the higher-order terms of m_{pole} . In the LL approximation ($\beta_0 > 0$, $\beta_1 = \beta_2 = \dots = 0$), similarly to the analysis of $V_{\text{QCD}}(r)$, the pole mass is given by

$$m_{\text{pole},\beta_0} = m_{\overline{\text{MS}}}(\mu) (1 + \delta_m), \quad (67)$$

$$\delta_m = \frac{C_F \alpha_s(\mu)}{2\pi} \sum_{n=0}^{\infty} \left[\frac{\beta_0 \alpha_s(\mu)}{4\pi} \right]^n \left[n! G_{n+1} + \frac{(-1)^n}{n+1} g_{n+1} \right]. \quad (68)$$

The expansion coefficients G_n and g_n are given in terms of generating functions as

$$\sum_{n=0}^{\infty} G_n u^n = \left(\frac{\mu^2}{m_{\overline{\text{MS}}}} \right)^u \times 3(1-u) \frac{\Gamma(1+u)\Gamma(1-2u)}{\Gamma(3-u)}, \quad (69)$$

$$\sum_{n=0}^{\infty} g_n y^n = \frac{3-2y}{6} \frac{\Gamma(4-2y)}{\Gamma(1+y)\Gamma(2-y)^2\Gamma(3-y)}. \quad (70)$$

The series with $n! G_{n+1}$ in eq. (68) includes renormalons. The contribution of the pole at $u = 1/2$ in $m_{\overline{\text{MS}}} \times \sum_n G_n u^n$ is proportional to $a^n n!$ with $a = \frac{\beta_0 \alpha_s}{2\pi}$. The proportionality coefficient is independent of $m_{\overline{\text{MS}}}$, by evaluating $m_{\overline{\text{MS}}} \times \left(\frac{\mu^2}{m_{\overline{\text{MS}}}} \right)^u$ at $u = 1/2$.

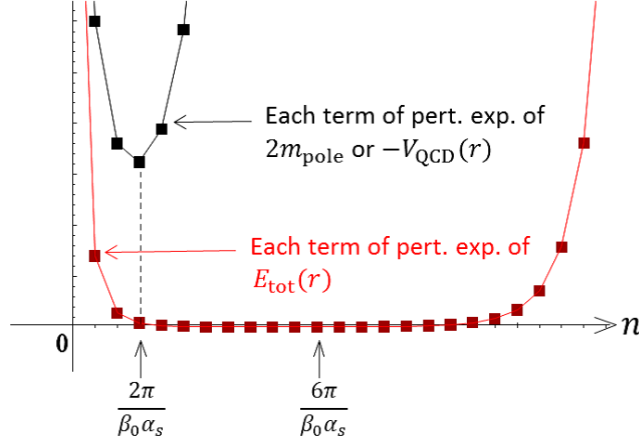
From the above result, we can estimate the uncertainty of the pole mass to be $\delta m_{\text{pole}} \sim \Lambda_{\text{QCD}} \sim 200\text{--}300$ MeV. In particular even if we take $m_{\overline{\text{MS}}}$ to zero, δm_{pole} remains to be order Λ_{QCD} , since δm_{pole} is independent of $m_{\overline{\text{MS}}}$. Then, one may wonder if it is a constituent quark mass of Sec. 2.1. We remark that this is not the case, in that δm_{pole} is an uncertainty and not a prediction.

Evaluating the residue at $u = 1/2$, one verifies that the uncertainties in $V_{\text{QCD}}(r)$ and m_{pole} cancel in the perturbative series of $E_{\text{tot}}(r)$. The IR renormalon pole of $E_{\text{tot}}(r)$ closest to the origin is at $u = 3/2$.* Namely, the convergence radius is enlarged. Consequently, convergence of the perturbative series of $E_{\text{tot}}(r)$ improves drastically compared

* For simplicity of the argument, let us ignore the contribution of the pole at $u = -1$ included in m_{pole} , which is a UV renormalon and gives a much less harmful sign-alternating series.

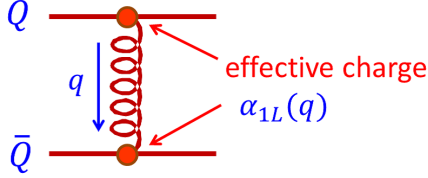
to those of $V_{\text{QCD}}(r)$ and m_{pole} individually. For this cancellation to happen, it is mandatory that (1) the uncertainty of $V_{\text{QCD}}(r)$ is independent of r , and that (2) the uncertainty of m_{pole} is independent of $m_{\overline{\text{MS}}}$. Both conditions are satisfied.

Let us examine the higher-order behavior of the perturbative series of $E_{\text{tot}}(r)$. Figure below shows schematically the renormalon estimates of higher-order terms of $2m_{\text{pole}}$ or $V_{\text{QCD}}(r)$ and $E_{\text{tot}}(r)$. The series converges more quickly and up to larger n for $E_{\text{tot}}(r)$.



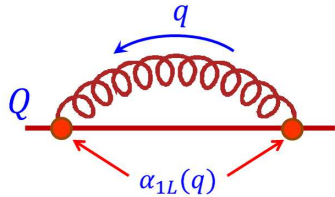
6.2 Mechanism of cancellation of IR contributions

We may understand qualitatively the mechanism of cancellation of the renormalons as follows. The potential and the pole mass in the LL approximation can be written as



$$V_{\beta_0}(r) = - \int \frac{d^3\vec{q}}{(2\pi)^3} e^{i\vec{q}\cdot\vec{r}} C_F \frac{4\pi\alpha_{1L}(q)}{q^2}, \quad (71)$$

$$m_{\text{pole},\beta_0} \simeq m_{\overline{\text{MS}}}(\mu) + \frac{1}{2} \int_{q<\mu} \frac{d^3\vec{q}}{(2\pi)^3} C_F \frac{4\pi\alpha_{1L}(q)}{q^2}. \quad (72)$$



$V_{\beta_0}(r)$ is essentially Fourier transform of the gluon propagator exchanged between quark and antiquark; the difference of m_{pole,β_0} and $m_{\overline{\text{MS}}}$ is essentially the infrared part of the quark self-energy. In both integrals, the charges are replaced by the one-loop running coupling constant $\alpha_{1L}(q)$. These are depicted schematically in the left figures.

As stated, the renormalon uncertainties stem from contributions from the region $q \lesssim \Lambda_{\text{QCD}}$ in the above integrals, where $\alpha_{1L}(q)$ is large. The signs of the renormalon contributions are opposite between $V_{\beta_0}(r)$ and m_{pole,β_0} , since the color charges are opposite between quark and antiquark while the self-energy is proportional to the square of the same charge. Their magnitudes differ by a factor of two because both the quark and

antiquark propagator poles contribute in the calculation of the potential, whereas only one of the two contributes in the calculation of the self-energy. Since we are concerned with a small q region, we may expand the Fourier factor in $V_{\beta_0}(r)$ in \vec{q} ,

$$e^{i\vec{q}\cdot\vec{r}} = 1 + i\vec{q}\cdot\vec{r} + \frac{1}{2}(i\vec{q}\cdot\vec{r})^2 + \dots \quad (73)$$

The leading term (=1) is canceled against $2m_{\text{pole},\beta_0}$, which corresponds to the renormalon at $u = 1/2$. In fact, integral of this term over the region $q \lesssim \Lambda_{\text{QCD}}$ ($\sim \int d^3\vec{q} 1/q^2$) evaluates to order Λ_{QCD} . The next term ($= i\vec{q}\cdot\vec{r}$) vanishes upon integration over \vec{q} , due to rotational invariance. The third term [$= \frac{1}{2}(i\vec{q}\cdot\vec{r})^2$] corresponds to the renormalon pole at $u = 3/2$ and is evaluated as

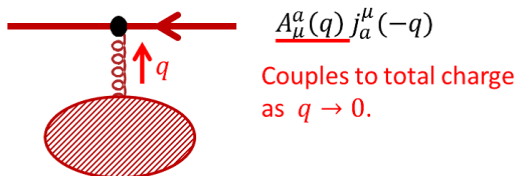
$$\delta V_{\beta_0}(r) \Big|_{\text{contr. of } u=3/2} \sim \int_{q \lesssim \Lambda_{\text{QCD}}} d^3\vec{q} (\vec{q}\cdot\vec{r})^2 \frac{1}{q^2} \sim \Lambda_{\text{QCD}} (\Lambda_{\text{QCD}} \cdot r)^2. \quad (74)$$

We obtain the same estimate if we perform an analysis similar to Sec. 5.2. This uncertainty from the $u = 3/2$ pole remains uncanceled.

Since the quark and antiquark are heavy, their typical distance r is small compared to the hadronization scale $\Lambda_{\text{QCD}}^{-1}$. Thus, the residual uncertainty $\Lambda_{\text{QCD}} (\Lambda_{\text{QCD}} \cdot r)^2$ is small compared to the original uncertainty Λ_{QCD} , since $r\Lambda_{\text{QCD}} \ll 1$.

Generally in perturbative QCD, convergence of perturbative series become worse at small energy scale. (e.g., the prediction of $V_{\text{QCD}}(r)$ at large r .) This is due to increase of contributions from IR gluons. Oppositely, if contributions from IR gluons are eliminated, perturbative series show better convergence behaviors.

The cancellation of IR contributions in $E_{\text{tot}}(r)$ is a general property of gauge theory, which holds beyond the LL approximation. This can be seen as follows. A static current has only the time component,



$$j_a^\mu(x) = T_a \delta^{\mu 0} \delta^3(\vec{x} - \vec{r}/2), \quad (75)$$

since a static color charge has no spatial motion. Hence, an IR gluon, which couples to static currents via minimal coupling $A_\mu^a(q) j_a^\mu(-q) =$

$A_0^a(q) j_a^0(-q)$, couples to the total charge of the system in the IR limit $q \rightarrow 0$:

$$Q_a^{\text{tot}} = \sum_{i=Q,\bar{Q}} j_{a,i}^0(q=0). \quad (76)$$

Therefore, an IR gluon decouples from a static color-singlet system. Diagrammatically,

however, an IR gluon can detect the total charge of the system only when both self-energy diagrams[†] and potential-energy diagrams are taken into account, as can be seen from the left figures. This means that a cancellation takes place between these two types of diagrams, since the gluon couples to individual diagrams but decouples from the sum of them.



Intuitively, IR gluons with wavelengths of order $\Lambda_{\text{QCD}}^{-1} (\gg r)$ cannot resolve the color charge of each particle, hence they only see the total charge of the system. More precisely, coupling of IR gluons to the system can be expressed by an expansion in \vec{r} (multipole expansion) for small r , in which the zeroth multipole (=total charge) of the color-singlet quark-antiquark pair is zero.

The modern approach (after around 1998) to use the $\overline{\text{MS}}$ mass for the computation of $E_{\text{tot}}(r)$ can be viewed as follows. The total energy of the system is computed as the sum of (i) the $\overline{\text{MS}}$ masses of Q and \bar{Q} , (ii) contributions to the self-energies of Q and \bar{Q} which are not included in the $\overline{\text{MS}}$ masses, and (iii) the potential energy between Q and \bar{Q} . Contributions of IR gluons with wavelengths larger than r automatically cancel between (ii) and (iii) in this computation. In this way we can eliminate IR contributions from the computation of $E_{\text{tot}}(r)$.

6.3 Perturbative prediction for $E_{\text{tot}}(r)$

Let us demonstrate the improvement of accuracy of the perturbative prediction for the total energy $E_{\text{tot}}(r) = 2m_{\text{pole}} + V_{\text{QCD}}(r)$ up to $\mathcal{O}(\alpha_s^3)$ (without using LL approximation). [Presently the perturbative series of $V_{\text{QCD}}(r)$ is known up to $\mathcal{O}(\alpha_s^4)$ and m_{pole} up to $\mathcal{O}(\alpha_s^3)$.]

As an example, we take the bottomonium case: We choose the $\overline{\text{MS}}$ mass of the b -quark, renormalized at the b -quark $\overline{\text{MS}}$ mass, as $\overline{m}_b \equiv m_b^{\overline{\text{MS}}}(m_b^{\overline{\text{MS}}}) = 4.190$ GeV; in internal loops, four flavors of light quarks are included with $\overline{m}_u = \overline{m}_d = \overline{m}_s = 0$ and $\overline{m}_c = 1.243$ GeV. In Fig. 10(a), we fix $r = 2.5$ GeV⁻¹ ≈ 0.5 fm and examine the μ -dependence of $E_{\text{tot}}(r)$, before rewriting $m_{b,\text{pole}}$ [Pole-mass scheme], and after rewriting $m_{b,\text{pole}}$ by \overline{m}_b [$\overline{\text{MS}}$ -mass scheme]. We see that $E_{\text{tot}}(r)$ is much less scale dependent when we use the $\overline{\text{MS}}$ mass (after cancellation of renormalons) than when we use the pole mass (before cancellation of renormalons). This shows clearly that the perturbative prediction of $E_{\text{tot}}(r)$ is much more stable if we use the $\overline{\text{MS}}$ mass.

We also compare the convergence behaviors of the perturbative series of $E_{\text{tot}}(r)$ for the same r and when μ is fixed to the scale where μ dependence vanishes (the minimal-sensitivity scale). At $r = 2.5$ GeV⁻¹, this scale is $\mu = 0.90$ GeV for the $\overline{\text{MS}}$ -mass scheme.

[†] In the large mass limit contributions from IR region to the pole mass approximate IR contributions to the self-energy of a static charge.

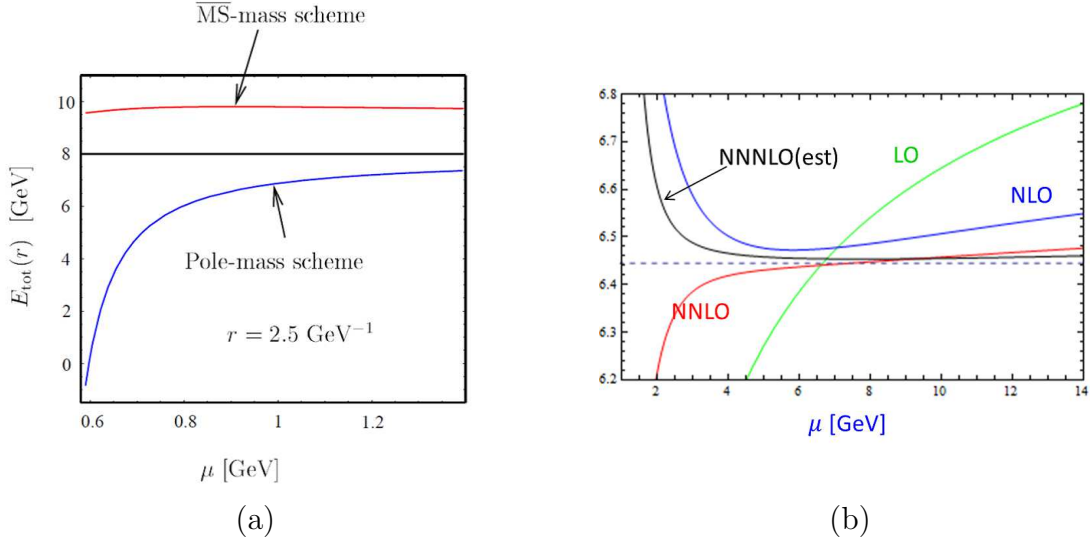


Figure 10: (a) Scale dependences of $E_{\text{tot}}(r)$ up to $\mathcal{O}(\alpha_s^3)$ at $r = 2.5 \text{ GeV}^{-1} \approx 0.5 \text{ fm}$, in the pole-mass and $\overline{\text{MS}}$ -mass schemes. (b) Scale dependences of $E_{\text{tot}}(r)$ at $r = 0.1 \text{ GeV}^{-1}$ in the $\overline{\text{MS}}$ -mass scheme at LO, NLO, NNLO and NNNLO. The NNNLO prediction uses the estimate by the large- β_0 approximation for the $\mathcal{O}(\alpha_s^4)$ term of the relation between the pole and $\overline{\text{MS}}$ masses. In both figures, horizontal lines are shown for guides.

Convergence of the series turns out to be close to optimal for this scale choice:[‡]

$$E_{\text{tot}}^{b\bar{b}}(r) = 10.408 - 0.275 - 0.362 - 0.784 \text{ GeV} \quad (\text{Pole-mass scheme}) \quad (77)$$

$$= 8.380 + 1.560 - 0.116 - 0.022 \text{ GeV} \quad (\overline{\text{MS}}\text{-mass scheme}). \quad (78)$$

The four numbers represent the $\mathcal{O}(\alpha_s^0)$, $\mathcal{O}(\alpha_s^1)$, $\mathcal{O}(\alpha_s^2)$ and $\mathcal{O}(\alpha_s^3)$ terms of the series expansion in each scheme. The $\mathcal{O}(\alpha_s^0)$ terms represent the twice of the pole mass and of the $\overline{\text{MS}}$ mass, respectively. The $\mathcal{O}(\alpha_s^1)$, $\mathcal{O}(\alpha_s^2)$, $\mathcal{O}(\alpha_s^3)$ terms in eq. (77) come solely from $V_{\text{QCD}}(r)$.

As can be seen, if we use the pole mass, the series is not converging beyond $\mathcal{O}(\alpha_s^1)$, whereas if we use the $\overline{\text{MS}}$ mass, the series is converging. One may further verify that, when the series is converging ($\overline{\text{MS}}$ -mass scheme), μ -dependence of $E_{\text{tot}}(r)$ decreases as we include more terms of the perturbative series, whereas when the series is diverging (pole-mass scheme), μ -dependence does not decrease with increasing order.

We observe qualitatively the same features at different r and for different number of light quark flavors n_f , or if we change the values of the masses \overline{m}_b , \overline{m}_c . Generally, at smaller r , $E_{\text{tot}}(r)$ becomes less μ -dependent and more convergent, due to the asymptotic freedom of QCD. See Fig. 10(b).

The stability against scale variation and convergence of the perturbative series are closely connected with each other. Formally, scale dependence vanishes at all order of

[‡] In the pole-mass scheme, there exists no minimal-sensitivity scale within a wide range of μ , and the convergence behavior of the series is qualitatively similar to eq. (77) within this range.

perturbation series. This means that, for a truncated perturbative series up to $\mathcal{O}(\alpha_s^N)$, scale dependence is of $\mathcal{O}(\alpha_s^{N+1})$. Hence, the scale dependence decreases for larger N as long as the series is converging. Thus, the truncated perturbative series is expected to become less μ -dependent with increasing order when the series is converging, and *vice versa*.

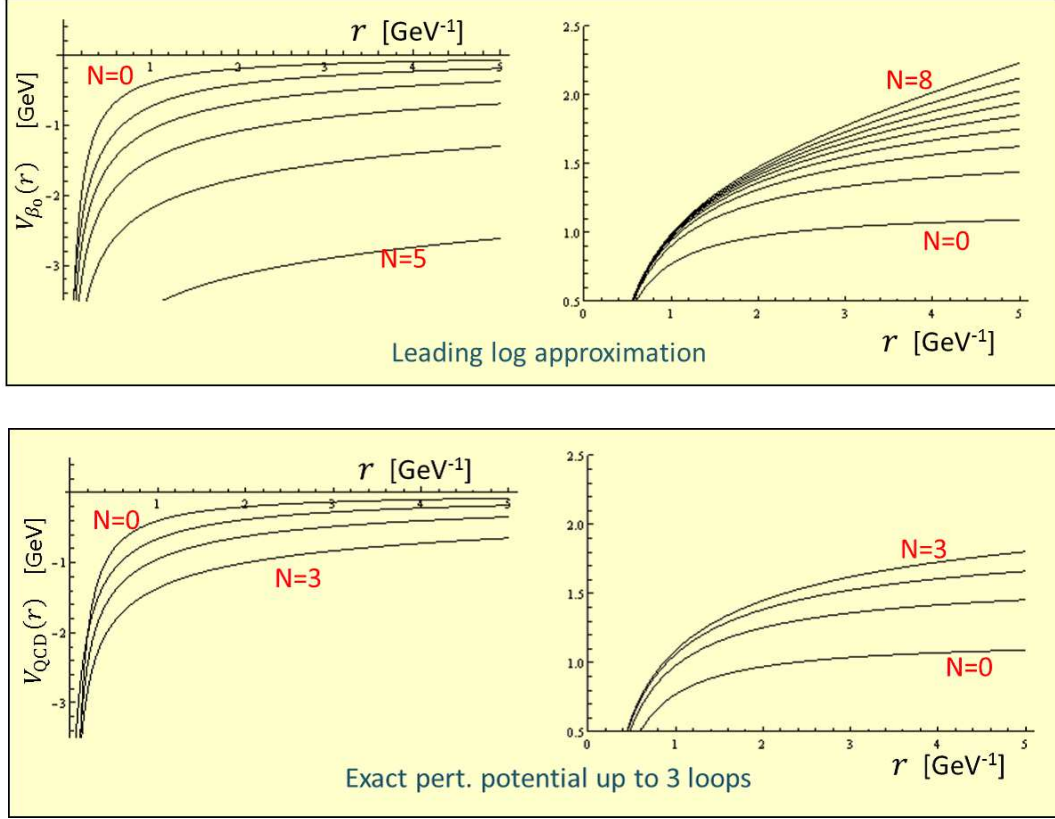


Figure 11: The potentials in the LL approximation and the exact perturbative potentials. (The former incorporates an improvement by the “large- β_0 approximation,” where μ is replaced by $\mu e^{5/6}$.) The potentials are given as the sum of the perturbative series up to $\mathcal{O}(\alpha_s^{N+1})$. We set $\mu = 2$ GeV, $\alpha_s = 0.3$ and $n_f = 4$ (all the internal quarks are taken to be massless). In the right figures, the dominant r -independent part [eq. (79)] is subtracted.

Finally we compare predictions of $V_{\text{QCD}}(r)$ in the LL approximation and exact perturbative series in Fig. 11. The left figures show the QCD potential truncated at $\mathcal{O}(\alpha_s^{N+1})$, while the right figures show the same potentials but after subtracting an r -independent $\mathcal{O}(\Lambda_{\text{QCD}})$ renormalon contribution

$$V_0^{(n)} = -C_F 4\pi\alpha_s \times \frac{\mu e^{5/6}}{2\pi^2} \left(\frac{\beta_0\alpha_s}{2\pi} \right)^n \times n! \quad (79)$$

from each term of the perturbative series. Compare eq. (61).[§]

[§] The replacement $\mu \rightarrow \mu e^{5/6}$ is incorporated in order to improve the estimate of the normalization

We see that the LL approximation gives good estimates of the known perturbative corrections. Convergence improves in the right figures. (Note that the vertical scale is magnified by factor two compared to the left figures, and also look in particular at the region $r \lesssim 2.5 \text{ GeV}^{-1} \approx 0.5 \text{ fm}$.) Furthermore, after subtracting the dominant r -independent part, the potential becomes steeper at larger r as we include more terms. This is a desirable feature, in the sense that it approaches the correct shape at larger r as we include higher-order terms, c.f. Sec. 4.1. (We collect some formulas for $E_{\text{tot}}(r)$ in Appendix A, such that one can reproduce the features demonstrated in this subsection.)

7 “Coulomb+Linear” Potential by Log Resummation

We have seen that, by including higher-order terms, $E_{\text{tot}}(r)$ becomes steeper at larger r (within the range $r < \Lambda_{\text{QCD}}^{-1}$). Numerically it approximates a “Coulomb+linear” shape. We show that a resummation of LLs, after subtracting renormalons, indeed leads to a “Coulomb+linear” potential.* This part of the potential is determined solely by UV contributions and is a genuine prediction of perturbative QCD.

There are two ways to derive the “Coulomb+linear” potential: one is based on resummation of LLs purely in perturbative prediction, the other uses the framework of a Wilsonian effective field theory (EFT). Both methods lead to the same formula. For pedagogical reasons, we explain the latter method in this lecture.

7.1 Analysis of $V_{\text{QCD}}(r)$ in an EFT framework (Outline)

We explain an outline of the analysis of $V_{\text{QCD}}(r)$ within a Wilsonian low energy EFT, called “potential-NRQCD (pNRQCD).” Its formulation will be explained extensively in Sec. 9. Here, we sketch some aspects in advance, required for the analysis in this section.

Let us first explain the general concept of a Wilsonian low energy EFT, written in terms of light quarks and gluons. Formally such an EFT can be constructed from full QCD by integrating out high-energy modes above a factorization scale $\mu_f (\gg \Lambda_{\text{QCD}})$, in a path-integral formulation of the theory. The Lagrangian of the EFT can be written in a form

$$\mathcal{L}_{\text{EFT}}(\mu_f) = \sum_i g_i(\mu_f) \mathcal{O}_i(\psi_q, \bar{\psi}_q, A_\mu), \quad (80)$$

which is a sum of operators \mathcal{O}_i composed of light quarks and gluons, whose energies and momenta are restricted to be below μ_f . The effective coupling constant $g_i(\mu_f)$ multiplying each operator is called a Wilson coefficient, which is determined such that physics at $E < \mu_f$ is unchanged from full QCD. Since the Wilson coefficients $g_i(\mu_f)$ ’s include only

of the renormalon using the so-called “large- β_0 approximation.” The potentials in the LL approximation in Fig. 11 are also improved by the same method. (This does not change the position of the renormalon poles in the Borel plane.)

* This can be extended to the cases NLL, NNLL, etc.

effects of UV degrees of freedom ($E > \mu_f$), they can be computed reliably using perturbative QCD. In practice there are two ways to compute the Wilson coefficients. One way is to compute various S matrix elements with external momenta of order E , where $\mu_f \gtrsim E \gg \Lambda_{\text{QCD}}$, in both EFT and full QCD in expansions in α_s , and to require that both computations give the same results. This is known as a matching procedure. The other method is to apply the technique called integration by regions, which determines the operators and Wilson coefficients of EFT in an efficient way by expanding Feynman diagrams in terms of small parameters. This method is explained briefly in Appendix C.

The Wilson coefficients computed using perturbative QCD should be free of uncertainties by IR renormalons, since the region of integration (above μ_f) does not include the domain where the strong coupling constant is large. Thus, the EFT Lagrangian eq. (80) consists of Wilson coefficients, which effectively contain information on UV degrees of freedom ($E > \mu_f$), and operators composed of dynamical variables representing IR degrees of freedom ($E < \mu_f$).

Generally a physical observable computed in the EFT is expressed by a sum of products of Wilson coefficients and matrix elements of IR operators. In this way we can factorize UV contributions (Wilson coefficients) and IR contributions (matrix elements which include non-perturbative contributions). If the observable includes a high mass scale $M (\gg \mu_f)$, the expression can be organized systematically in an expansion in powers of $1/M$. Since matrix elements of operators include scales only below μ_f , this expansion generates powers of small parameters ($\lesssim \mu_f/M$). As compared to the purely perturbative computation of the same observable, in the EFT formulation, only UV part of the purely perturbative prediction is encoded in the Wilson coefficients, whereas uncertainties originating from IR renormalons in perturbative QCD are replaced by non-perturbative matrix elements. Hence, intrinsic uncertainties are eliminated from perturbative computations of the Wilson coefficients, and we obtain more accurate predictions as we compute higher-orders corrections (provided that non-perturbative matrix elements can be determined in some way).

In the case of the static QCD potential, since the perturbative prediction is more accurate at short distances, $r \ll \Lambda_{\text{QCD}}^{-1}$, we consider a short-distance expansion of $V_{\text{QCD}}(r)$:

$$V_{\text{QCD}}(r) \sim \frac{c_{-1}}{r} + c_0 + c_1 r + c_2 r^2 + \dots \quad (81)$$

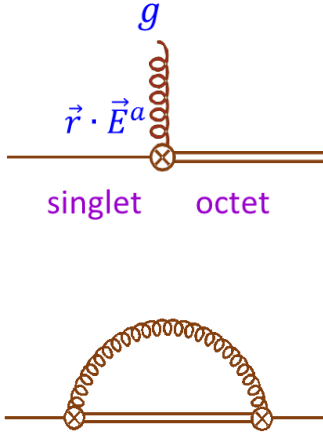
This expansion in r is (at best) qualitative, in the sense that there must be a logarithmic correction at least to the Coulomb term $\sim 1/[r \log(\Lambda_{\text{QCD}} r)]$, as designated by the renormalization-group equation. We have seen in previous sections that, in purely perturbative evaluation of $V_{\text{QCD}}(r)$, the leading uncertainty at $r \ll \Lambda_{\text{QCD}}^{-1}$ is included in the r -independent constant, while the next-to-leading uncertainty is included in the r^2 term, induced by the renormalons:

$$c_0 \sim \mathcal{O}(\Lambda_{\text{QCD}}), \quad (82)$$

$$c_2 r^2 \sim \mathcal{O}(\Lambda_{\text{QCD}}^3 r^2). \quad (83)$$

The renormalon in c_0 is canceled against the renormalon in $2m_{\text{pole}}$ in the total energy $E_{\text{tot}}(r)$. The renormalon in c_2 is replaced by a non-perturbative matrix element if we compute $E_{\text{tot}}(r)$ in the pNRQCD EFT framework.

pNRQCD is a low energy EFT which describes interaction between a heavy $Q\bar{Q}$ system and IR gluons. In this EFT, IR gluons, whose wavelengths are larger than r ,



interact with color multipoles of the $Q\bar{Q}$ system. Since the color charge of a $Q\bar{Q}$ bound state is zero (color singlet), the leading interaction of the singlet bound state with IR gluons is a dipole-type, $\vec{r} \cdot \vec{E}^a$, where \vec{E}^a denotes the color electric field. This is depicted as a vertex of pNRQCD in the left figure.

The leading contribution to the $Q\bar{Q}$ bound state energy from IR degrees of freedom is given by the self-energy diagram with two insertions of the dipole interactions (see the left figure), which is expressed in terms of the matrix element

$$\langle \vec{r} \cdot \vec{E}^a(t) \vec{r} \cdot \vec{E}^a(0) \rangle. \quad (84)$$

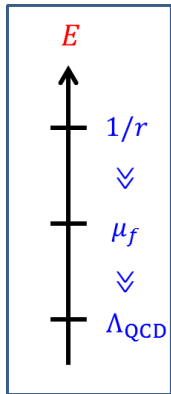
We will see in Sec. 9 that it has a correct form to replace the $\mathcal{O}(r^2)$ renormalon in the purely perturbative prediction.

7.2 UV contributions to $V_{\text{QCD}}(r)$ and OPE

Let us use the framework of pNRQCD with a factorization scale μ_f to compute $V_{\text{QCD}}(r)$. We assume

$$r^{-1} \gg \mu_f \gg \Lambda_{\text{QCD}}. \quad (85)$$

In this framework the Wilson coefficient, which corresponds to the UV contribution to $V_{\text{QCD}}(r)$, can be computed using perturbative QCD. We introduce a cut-off in the momentum-space integral and resum LLs:



$$V_{\text{UV}}(r; \mu_f) \equiv - \int_{q > \mu_f} \frac{d^3 \vec{q}}{(2\pi)^3} e^{i\vec{q} \cdot \vec{r}} C_F \frac{4\pi \alpha_{1\text{L}}(q)}{q^2}, \quad (86)$$

where

$$\alpha_{1\text{L}}(q) = \frac{2\pi}{\beta_0 \log(q/\Lambda_{\text{QCD}})}. \quad (87)$$

The integral is well defined, since the pole of $\alpha_{1\text{L}}(q)$ is not included in the integral region.

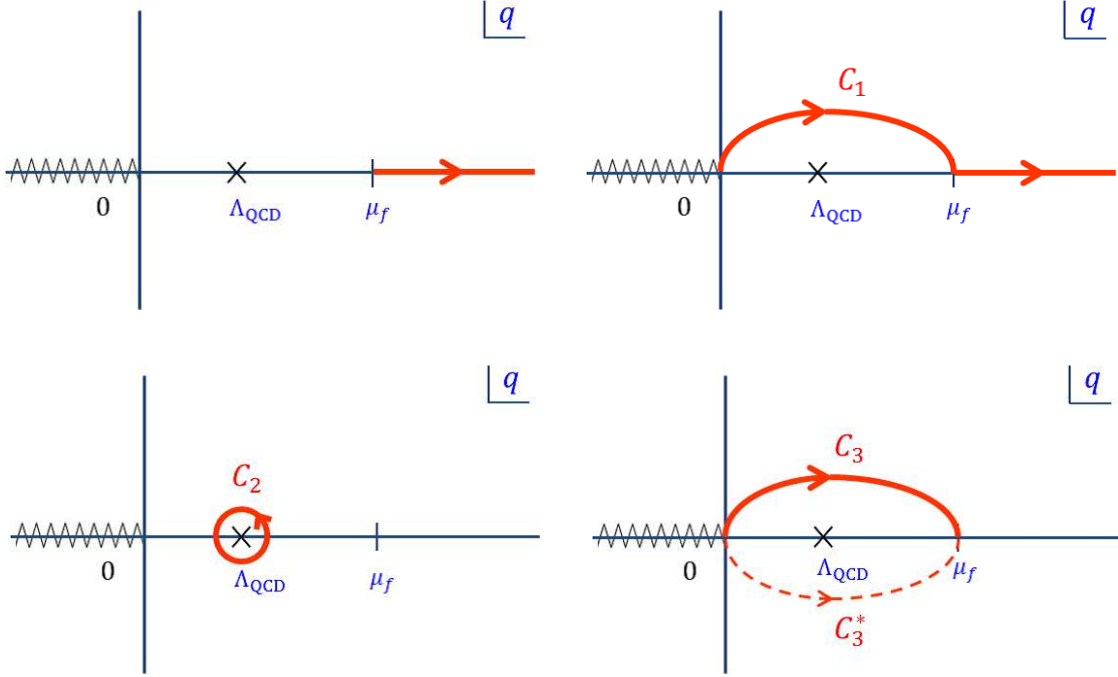


Figure 12: Integral contours in the complex q -plane shown by red lines. C_3^* (dashed line) represents the complex conjugate of C_3 . A pole and branch cut of the integrand are also shown.

We can obtain a short-distance expansion of V_{UV} as follows. After integrating over the angular variables, we obtain a one-parameter integral

$$V_{UV}(r; \mu_f) = -\frac{2C_F}{\pi} \int_{\mu_f}^{\infty} dq \frac{\sin(qr)}{qr} \alpha_{1L}(q) = -\frac{2C_F}{\pi} \text{Im} \int_{\mu_f}^{\infty} dq \frac{e^{iqr}}{qr} \alpha_{1L}(q). \quad (88)$$

This is an integral along the real axis in the complex q -plane, ranging from $q = \mu_f$ to $q = \infty$. We separate the integral contour into the difference of two contours $C_1 - C_3$ in the complex q -plane; see Fig. 12. Since $\mu_f r \ll 1$, along the contour C_3 it is justified to expand the Fourier factor as

$$e^{iqr} = 1 + iqr + \frac{1}{2}(iqr)^2 + \dots. \quad (89)$$

Then the integral along C_3 can be written as

$$\frac{2C_F}{\pi} \text{Im} \int_{C_3} dq \frac{1 + iqr + \frac{1}{2}(iqr)^2 + \dots}{qr} \alpha_{1L}(q) = \frac{A}{r} + B + \sigma r + Dr^2 + \mathcal{O}(r^3). \quad (90)$$

The coefficient A can be computed analytically as[†]

$$\begin{aligned} A &= \frac{2C_F}{\pi} \text{Im} \int_{C_3} dq \frac{\alpha_{1L}(q)}{qr} = \frac{C_F}{\pi i} \int_{C_3 - C_3^*} dq \frac{\alpha_{1L}(q)}{qr} \\ &= -\frac{C_F}{\pi i} \int_{C_2} dq \frac{\alpha_{1L}(q)}{qr} = -\frac{4\pi C_F}{\beta_0}. \end{aligned} \quad (91)$$

The integral contour can be deformed to C_2 , which surrounds the pole of $\alpha_{1L}(q)$. Then we used the Cauchy theorem in the last equality.

We can evaluate the coefficient σ in a similar manner:

$$\sigma = \frac{2C_F}{\pi} \text{Im} \int_{C_3} dq \left(-\frac{1}{2}q\right) \alpha_{1L}(q) = \frac{C_F}{2\pi i} \int_{C_2} dq q \alpha_{1L}(q) = \frac{2\pi C_F}{\beta_0} \Lambda_{\text{QCD}}^2. \quad (92)$$

Although originally the expressions for A and σ appear to be dependent on μ_f , in fact they reveal to be independent of μ_f , since they can be expressed by integrals along the closed contour C_2 .

In contrast, B and D are dependent on μ_f , since they cannot be expressed as integrals along a closed contour:[‡]

$$B = \frac{2C_F}{\pi} \text{Re} \int_{C_3} dq \alpha_{1L}(q), \quad (93)$$

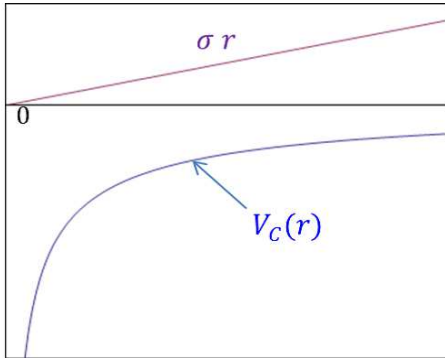
$$D = -\frac{C_F}{3\pi} \text{Re} \int_{C_3} dq q^2 \alpha_{1L}(q). \quad (94)$$

Combining these, we obtain

$$V_{\text{UV}}(r; \mu_f) = V_C(r) + B + \sigma r + Dr^2 + \mathcal{O}(r^3), \quad (95)$$

$$V_C(r) = \frac{A}{r} - \frac{2C_F}{\pi} \text{Im} \int_{C_1} dq \frac{e^{iqr}}{qr} \alpha_{1L}(q). \quad (96)$$

Note that $V_C(r)$ is independent of μ_f , since the integral along C_1 is also independent of the intermediate point μ_f . $V_C(r)$ and σr are shown in the left figure. The asymptotic behaviors of $V_C(r)$ as $r \rightarrow 0$ and $r \rightarrow \infty$ can be computed analytically as



$$V_C(r) \rightarrow \begin{cases} -\frac{2\pi C_F}{\beta_0} \frac{1}{r |\log(\Lambda_{\text{QCD}} r)|}, & r \rightarrow 0, \\ -\frac{4\pi C_F}{\beta_0 r}, & r \rightarrow \infty. \end{cases} \quad (97)$$

[†] Note that $\alpha_{1L}(q)^* = \alpha_{1L}(q^*)$ in the domain $\text{Re } q > 0$ according to eq. (87).

[‡] The difference is that the integrals can be written only as ones along $C_3 + C_3^*$ rather than $C_3 - C_3^*$.

[See Appendix B for computation of $V_C(r)$.] At $r \rightarrow 0$, $V_C(r)$ tends to a Coulomb potential with the correct logarithmic correction as determined by the RG equation; at $r \rightarrow \infty$, it approaches a pure Coulomb potential; in the intermediate distance region these asymptotic behaviors are smoothly interpolated. Thus, eq. (95) can be regarded as a (qualitative) expansion of $V_{UV}(r)$ in r , at short-distances.

As will be shown in Sec. 9, the operator-product expansion (OPE) of $V_{QCD}(r)$ in r within pNRQCD framework takes a form

$$V_{QCD}(r) = V_{UV}(r; \mu_f) + V_{IR}(r; \mu_f), \quad (98)$$

where the leading term of the IR contribution V_{IR} is expressed in terms of the non-perturbative matrix element of eq. (84). Substituting the expansion (95), we obtain

$$V_{QCD}(r) = \text{const.} + \underbrace{V_C(r) + \sigma r}_{\mu_f\text{-indep.}} + \underbrace{Dr^2 + V_{IR}^{(LO)}(r; \mu_f)}_{\mu_f\text{-indep.}} + \mathcal{O}(r^3). \quad (99)$$

We can show explicitly that the μ_f -dependences cancel between Dr^2 and the leading non-perturbative contribution (see Sec. 9.7). It is consistent, since in total $V_{QCD}(r)$ should be independent of the factorization scale μ_f . We also note that, if the ‘‘Coulomb’’ and linear terms were dependent on μ_f , that would have led to inconsistencies, since there are no IR contributions which can cancel such μ_f -dependences.

Thus, $V_C(r) + \sigma r$ is included in a short-distance expansion of $V_{UV}(r; \mu_f)$ and insensitive to μ_f . Therefore, it is a genuinely UV contribution, determined by perturbative QCD.[§] We also emphasize that, since σr arises in the short-distance expansion, a priori this linear potential has nothing to do with the linear potential as determined from the large-distance behavior of $V_{QCD}(r)$, which is closely connected with quark confinement.

We show (without derivation) the result of analysis including subleading logarithms via RG equation. Fig. 13 shows a comparison of lattice data and $V_C(r) + \sigma r$ in different orders of log resummations. As can be seen, with increasing order, the range where $V_C(r) + \sigma r$ (perturbative prediction) agrees with the lattice data extends to larger r . The difference between the lattice computations and the purely perturbative computation corresponds to the ‘‘ $\mathcal{O}(r^2)$ -term,’’ $Dr^2 + V_{IR}^{(LO)}(r; \mu_f)$, up to higher-order terms in r . At NNNLL, there is no room in this difference to accommodate a linear potential Kr of eq. (30) at $r \lesssim 0.5$ fm. Namely, one should not add a linear term to the perturbative potential in this region. To our current knowledge, σ increases as we include more subleading logarithms. For example, at NNNLL and $n_f = 0$, σ/K is between 1/3 and 1/2, where K is determined from the large-distance behavior of $V_{QCD}(r)$ by lattice computations.

As mentioned, it is not essential to introduce the factorization scale μ_f to derive the ‘‘Coulomb+linear’’ potential. It can be shown that the truncated series expansion of

[§] We are not concerned about the constant part of $V_{QCD}(r)$, since it is also dominated by UV contributions when combined with $2m_{\text{pole}}$ in $E_{\text{tot}}(r)$.

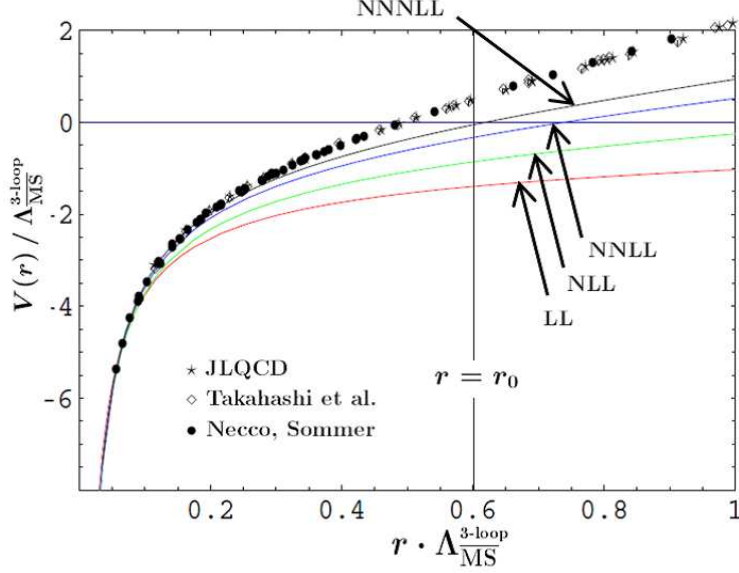


Figure 13: Comparison of lattice computations of $V_{\text{QCD}}(r)$ (data points) and perturbative QCD predictions for $V_C(r) + \sigma r$ (solid lines) in the case $n_f = 0$ (quenched approximation). r_0 denotes the Sommer scale, which is considered to be roughly $0.5 \text{ fm} \approx (400 \text{ MeV})^{-1}$.

$E_{\text{tot}}(r)$,

$$\sum_{n=0}^N \left[2m_{\text{pole}, \beta_0}^{(n)} + V_{\beta_0}^{(n)}(r) \right] \quad \text{for } N < n_0 = \frac{6\pi}{\beta_0 \alpha_s}, \quad (100)$$

approaches toward $V_C(r) + \sigma r$, up to an uncertainty $\sim \text{const.} + \mathcal{O}(\Lambda_{\text{QCD}}^3 r^2)$ (c.f., Sec. 6.1).

Let us present an interpretation of the formula for $V_C(r) + \sigma r$, eqs. (91), (92) and (96). The integral contours in these formulas originate from a relation depicted schematically as below:

This has a form where contributions from IR region are subtracted as contour integrals surrounding the pole at $q = \Lambda_{\text{QCD}}$. Hence, it can be regarded as a generalization of the method of “integration by regions,” in which contributions from different scales are factorized as contour integrals surrounding the corresponding poles in each Feynman diagram. (See Appendix C.) In computing $V_{\text{UV}}(r; \mu_f)$ we need to separate UV and IR contributions in $V_{\text{QCD}}(r)$ and subtract the latter. It is, however, not possible to identify IR contributions by the standard integration-by-regions technique, since the scale Λ_{QCD} never appears as a singularity at each order of perturbative expansion. In our formula, the scale Λ_{QCD} appears as a singularity by log resummation, and its contributions are subtracted as contour integrals.

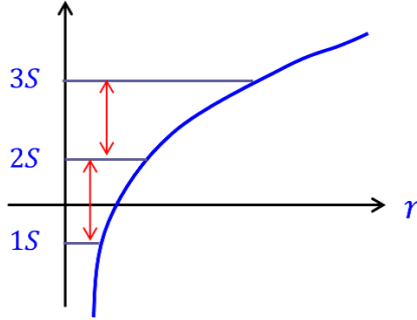


Figure 14: A schematic diagram showing the energy levels of the Hamiltonian Eq. (102). The level spacings are order $\Lambda_{\text{QCD}}(\Lambda_{\text{QCD}}/m)^{1/3}$ if they are predominantly determined by the linear part σr of the potential.

8 Implication and Interpretation

Using the result of the previous section, we can compute the total energy of a static $Q\bar{Q}$ pair as

$$E_{\text{tot}}(r) = 2\bar{m} + \text{const.} + V_C(r) + \sigma r + \mathcal{O}(\Lambda_{\text{QCD}}^3 r^2) \quad (101)$$

within perturbative QCD, where the r -independent part is also UV dominant and accurately predictable. (The $\mathcal{O}(\Lambda_{\text{QCD}}^3 r^2)$ uncertainty can be replaced by a non-perturbative matrix element within the EFT approach.) The spectrum of a heavy quarkonium system, such as bottomonium, can be computed roughly as the energy eigenvalues of the quantum mechanical Hamiltonian*

$$H = \frac{\vec{p}^2}{m_{\text{pole}}} + E_{\text{tot}}(r). \quad (102)$$

A linear potential of order $\Lambda_{\text{QCD}}^2 r$ generates level spacings between different S -states of order $\Lambda_{\text{QCD}}(\Lambda_{\text{QCD}}/m)^{1/3}$.[†] On the other hand, a Coulomb potential $\sim -\alpha_s/r$ generates level spacings of order $\alpha_s^2 m$. For the bottomonium states, the linear potential is estimated to be comparable to or more important than the Coulomb potential in generating these level spacings. In contrast, if we consider (would-be) toponium states, the Coulomb potential by far dominates over the linear potential. Thus, a major part of the perturbative QCD predictions for the level spacings between different bottomonium S -states is order $\Lambda_{\text{QCD}}(\Lambda_{\text{QCD}}/m)^{1/3}$. See Fig. 14.

We may develop a microscopic understanding on the composition of the energy of a bottomonium state, using eqs. (71) and (72). After integration over angular variables,

* More accurate prediction is possible using the potential-NRQCD framework. Currently the spectrum is known up to NNNLO.

[†] This estimate can be derived using a semi-classical approximation (WKB approximation) in quantum mechanics.

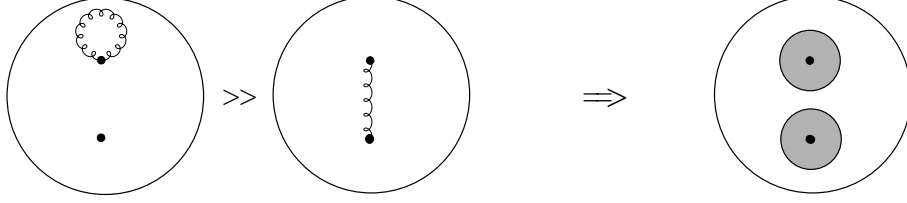


Figure 15: The total energy of a heavy quarkonium state is carried by the $\overline{\text{MS}}$ masses of Q and \bar{Q} and by the gluons whose wavelengths are smaller than the bound-state size. In the latter contributions the self-energies of Q and \bar{Q} dominate over the potential energy between the two particles.

we obtain

$$2m_{\text{pole}} \approx 2m_{\overline{\text{MS}}}(\mu) + \frac{2C_F}{\pi} \int_0^\mu dq \alpha_{1L}(q), \quad (103)$$

$$V_{\text{QCD}}(r) \approx -\frac{2C_F}{\pi} \int_0^\infty dq \frac{\sin(qr)}{qr} \alpha_{1L}(q). \quad (104)$$

For a bottomonium state X ,

$$\begin{aligned} E_X^{b\bar{b}} &= \langle X | \hat{H} | X \rangle \\ &\approx \langle X | \frac{\vec{p}^2}{m_{\text{pole}}} + 2m_{\overline{\text{MS}}}(\mu) + \frac{2C_F}{\pi} \int_0^\mu dq \alpha_{1L}(q) - \frac{2C_F}{\pi} \int_0^\infty dq \frac{\sin(qr)}{qr} \alpha_{1L}(q) | X \rangle \\ &= 2m_{\overline{\text{MS}}}(\mu) + \langle X | \frac{\vec{p}^2}{m_{\text{pole}}} | X \rangle + \frac{2C_F}{\pi} \int_0^\infty dq \alpha_{1L}(q) f_X(q), \end{aligned} \quad (105)$$

where

$$f_X(q) = \theta(\mu - q) - \int_0^\infty dr r^2 |R_X(r)|^2 \frac{\sin(qr)}{qr}. \quad (106)$$

$R_X(r)$ represents the radial part of the wave function of X . We find that the kinetic energy $\langle X | \vec{p}^2/m_{\text{pole}} | X \rangle$ turns out to be numerically small, which we ignore in the following discussion.[‡]

Let us set $\mu = m_{\overline{\text{MS}}}(\mu) (\equiv \bar{m}_b)$ for the bottomonium case. According to the discussion in Sec. 6.2, infrared gluons decouple in the computation of the energy of a bottomonium state X . The energy consists of the self-energies of b and \bar{b} and the potential energy between b and \bar{b} , where gluons whose wavelengths λ are smaller than the bound state size a_X contribute. At IR ($\lambda > a_X$) the sum of the self-energies and the potential energy cancel. On the other hand, at UV ($\lambda < a_X$), the potential energy quickly dumps due

[‡] This does not contradict the virial theorem for the Coulomb system, since our potential is significantly deviated from the Coulomb potential.

to the rapid oscillation factor $e^{i\vec{q}\cdot\vec{r}}$ for large q in the potential energy. See eqs. (71) and (72). It means that the major contribution to the bottomonium energy comes from the region (in momentum space) $1/a_X \lesssim q \lesssim \bar{m}_b$ of the self-energy corrections of b and \bar{b} , apart from the constant contribution $2\bar{m}_b$. See Fig. 15.

In fact, the composition of the energy in momentum space, eq. (105) when $\langle p^2/m \rangle$ is neglected, has exactly this form, since $f_X(q)$ is a support function constructed from the wave function of the bound state X , which is roughly unity in the region $1/a_X \lesssim q \lesssim \bar{m}_b$; see Fig. 16(a).

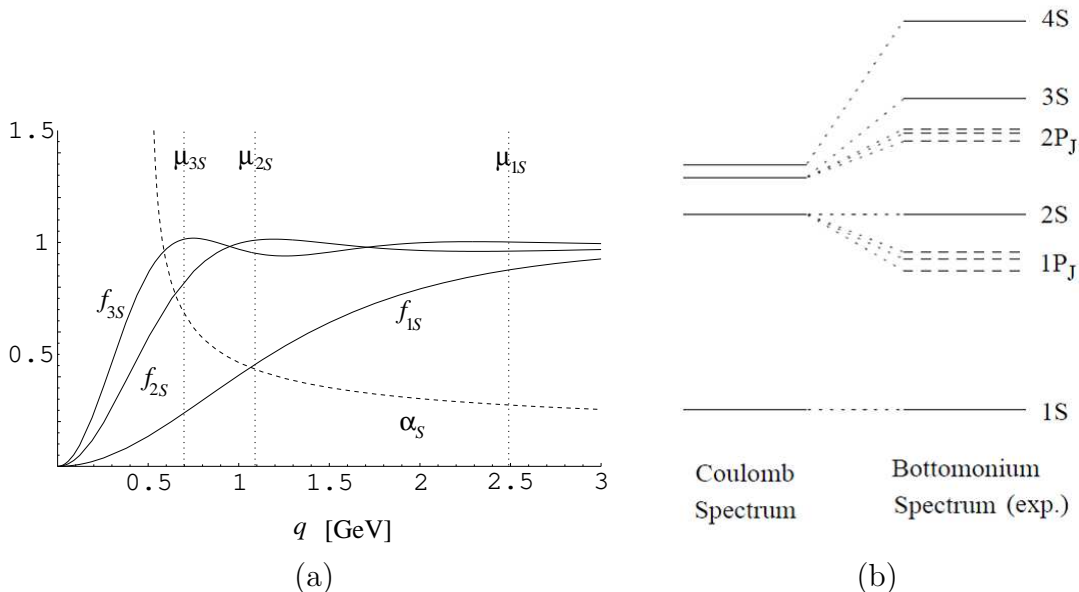


Figure 16: (a) The support functions $f_X(q)$ used to express the energy of the bottomonium state X in Eq. (105) for $X = 1S, 2S$ and $3S$. The running coupling constant $\alpha_s(q)$ close to the dumping scale of $f_X(q)$ grows rapidly as X varies from the $1S$ to $3S$ states. μ_X represents the typical momentum scale of X . (b) Comparison of the Coulomb spectrum and observed bottomonium spectrum. The Coulomb spectrum is scaled such that the $1S$ - $2S$ level spacing coincides with that of the bottomonium spectrum.

A characteristic feature of the bottomonium spectrum in comparison to the Coulomb spectrum is that the level spacings among the bottomonium excited states are much wider than those of the Coulomb spectrum. The level spacings of the Coulomb spectrum shrink quickly for higher levels. The difference from the Coulomb spectrum results from the linear rise of the potential. See Figs. 14 and 16(b).

The size a_X of the state X becomes larger for higher excited states. Then gluons with longer wavelengths can contribute to the energy of X . Positive contributions to the self-energies increase rapidly since interactions of IR gluons become stronger by the running of the coupling constant. In Fig. 16(a) also $\alpha_s(q)$ is shown. We see that as the state varies from $X = 1S$ to $3S$, the coupling $\alpha_s(q)$, close to the dumping scale of $f_X(q)$,

grows rapidly. According to Eq. (105), as the integral region extends down to smaller q , the self-energy contributions grow rapidly in comparison to the non-running case. (Note that the non-running case corresponds to the Coulomb spectrum.) The self-energies push up the energy levels of the excited states considerably and widen the level spacings among the excited states as compared to the Coulomb case.

Hence, we may draw the following qualitative pictures for the energies of the bottomonium states:

- (I) The energy of a bottomonium state mainly consists of (i) the $\overline{\text{MS}}$ masses of b and \bar{b} ($= 2\overline{m}_b$), and (ii) contributions to the self-energies of b and \bar{b} from gluons with wavelengths $1/\overline{m} \lesssim \lambda_g \lesssim a_X$. The latter contributions may be regarded as the difference between the (state-dependent) constituent quark masses and the current quark masses.
- (II) The energy levels between excited states are widely separated as compared to the Coulomb spectrum. This is because the self-energy contributions (from $1/\overline{m} \lesssim \lambda_g \lesssim a_X$) grow rapidly as the physical size a_X of the bound-state increases.

We conjecture that the conventional picture, that the mass of a light hadron consists of the constituent quark masses, can be viewed as an extrapolation of picture (I), although it lies outside the validity range of perturbative QCD. An important point is that it is clear in perturbative QCD to which extent the prediction can be made quantitative. Namely, the potential energy is predictable up to the linear potential $\sim \Lambda_{\text{QCD}}^2 r$ [corresponding to the bound state energy $\sim \Lambda_{\text{QCD}}(\Lambda_{\text{QCD}}/m_Q)^{1/3}$], while the quadratic potential $\sim \Lambda_{\text{QCD}}^3 r^2$ cannot be predicted.

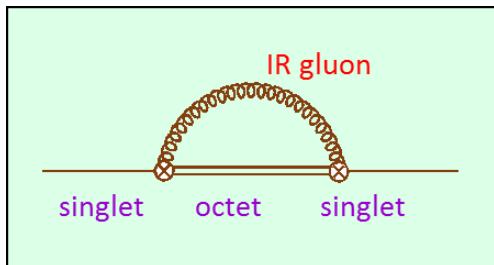
9 Potential-NRQCD EFT in Static Limit

As already mentioned in Sec. 7.1, pNRQCD is an EFT appropriate for describing interactions between a static quark-antiquark system and IR gluons. In fact, Wilsonian low energy EFTs can be constructed from full QCD particularly clearly for this system, and one can trace a number of steps in perturbative expansions in α_s .

In this section we mainly explain the construction and structure of the EFT when we integrate out the scale $1/r$. We clarify how the renormalon is replaced by a non-perturbative matrix element. We also discuss briefly the case where the binding energy scale $\sim -\alpha_s/r$ is further integrated out.

9.1 Historical background

Soon after the birth of perturbative QCD, it was pointed out that perturbative series of $V_{\text{QCD}}(r)$ contains IR divergences starting from three-loop order (Appelquist, Dine,



Muzunich). The IR divergences originate from degeneracy of the energy of the initial- or final-state with those of intermediate states. At the same time, the divergences are unique to the non-abelian gauge theory and is absent in QED. Consider a process as depicted in the left figure: the color-singlet static $Q\bar{Q}$ pair emits and re-

absorbs an IR gluon; in the intermediate state, the $Q\bar{Q}$ pair turns to a color-octet state due to color conservation. According to time-independent perturbation theory, this process contributes to the energy of the system as

$$\delta V_{\text{QCD}}(r) \sim \sum_{\vec{k}_g} \frac{|\langle S | H_{\text{int}} | Og \rangle|^2}{(E_O + |\vec{k}_g|) - E_S} = \sum_{\vec{k}_g} \frac{|\langle S | H_{\text{int}} | Og \rangle|^2}{|\vec{k}_g| + \Delta V}, \quad (107)$$

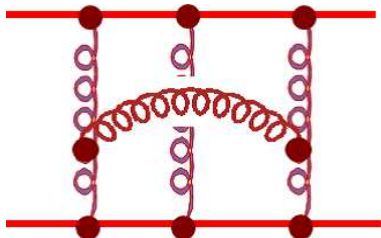
where

$$E_S = V_S(r) = -C_F \frac{\alpha_s}{r} + \mathcal{O}(\alpha_s^2), \quad (108)$$

$$E_O = V_O(r) = \left(\frac{C_A}{2} - C_F \right) \frac{\alpha_s}{r} + \mathcal{O}(\alpha_s^2), \quad (109)$$

$$\Delta V = E_O - E_S = \frac{C_A}{2} \frac{\alpha_s}{r} + \mathcal{O}(\alpha_s^2) \quad (110)$$

denote, respectively, the energy of the singlet state, that of the octet state, and the difference of the two energies. (The Casimir operator for the adjoint representation is defined by $T_{\text{adj}}^a T_{\text{adj}}^a = C_A \mathbf{1}$, and $C_A = 3$ for QCD.)



In eq. (107), if we expand $(|\vec{k}_g| + \Delta V)^{-1}$ in $\Delta V \propto \alpha_s$, we find that an IR divergence emerges corresponding to the three-loop diagram shown in the left figure. If we retain ΔV in the denominator, it becomes IR finite. Thus, the energy difference between the initial (final) and intermediate states regularizes the divergence, if we do not expand in α_s . We may compare this feature with

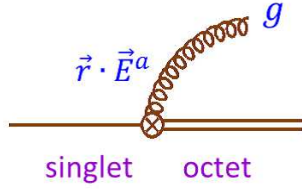
the collinear divergence in the process where an electron emits a photon: if the electron propagator $(p_e^2 - m_e^2)^{-1}$ is expanded in m_e , the electron self-energy diagram exhibits a collinear divergence, while it behaves as $\log(E_e/m_e)$ if we do not expand in m_e .*

The above argument indicates existence of a non-trivial IR dynamics in this system, and pNRQCD is suited to clarify its nature. It is also closely related to the Lamb shift in QED bound states.

* The IR divergences in $V_{\text{QCD}}(r)$ are different from the usual IR divergences which cancel between virtual corrections and real emission processes according to Kinoshita-Lee-Nauenberg theorem, since there are no real emission processes contributing to $V_{\text{QCD}}(r)$. The mechanism for the absence of IR divergence is closer to that of the collinear divergence for finite electron mass, as described here.

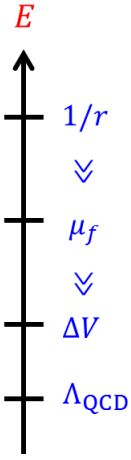
9.2 Basic concept of pNRQCD for static quarks

We consider a system composed of a static $Q\bar{Q}$ pair and IR gluons.[†] We assume that $1/r \gg \Delta V(r)$ [‡] and simultaneously energies of IR gluons satisfy $E_g \lesssim \Delta V(r)$.



The EFT describes dynamics such as the one shown in the left figure, namely the $Q\bar{Q}$ system emits or absorbs IR gluons whose energies are comparable to or smaller than energy differences of different $Q\bar{Q}$ states. We choose the factorization scale μ_f as

$$\Delta V(r) \ll \mu_f \ll \frac{1}{r} \quad (111)$$



and integrate out dynamical degrees of freedom above the scale μ_f . The assumed scale hierarchy is shown in the left figure.

The dynamical degrees of freedom of the EFT, which remain after integrating out the higher modes, are written in terms of the following quantum fields:

$$Q\bar{Q} \text{ composite fields } \begin{cases} \text{color-singlet field : } S(\vec{X}, \vec{r}; t), \\ \text{color-octet field : } O(\vec{X}, \vec{r}; t), \end{cases} \quad (112)$$

$$\text{IR gluon : } A_0(t, \vec{x}), \vec{A}(t, \vec{x}). \quad (113)$$

We denote the positions of Q and \bar{Q} as $\vec{X} \pm \vec{r}/2$, namely, \vec{X} stands for the c.m. coordinate of Q and \bar{Q} , while \vec{r} stands for the relative coordinate.

The $Q\bar{Q}$ composite fields are bilocal in space coordinates but local in time coordinate.

The expansion parameters of this EFT are as follows.

- (i) Since $rE_g = rp_g \ll 1$, the time and spatial derivatives acting on gauge fields, such as $\vec{r} \cdot \partial_t \vec{A}$ and $\vec{r} \cdot \vec{\partial} A_0$, are considered as “small.” These are induced by multipole expansion of $A_\mu(t, \vec{X} \pm \vec{r}/2)$ in \vec{r} .

Intuitively, since IR gluons have long wavelengths, $\lambda_g (= E_g^{-1}) \gg r$, they cannot resolve internal structures of the $Q\bar{Q}$ state but rather couple to color multipoles.

- (ii) On the other hand, since $rp_r \sim \mathcal{O}(1)$ by uncertainty principle, we do not expand the $Q\bar{Q}$ fields S and O in \vec{r} .
- (iii) Since $rE_{S,O} \sim r\Delta V \ll 1$, expansions such as $(r\partial_t)^n S$ are legitimate. Nevertheless, we can eliminate more than one time derivative ∂_t acting on S or O using the equation of motion.

[†]We may also include massless quarks, which can be treated similarly to gluons.

[‡]This is equivalent to $\frac{1}{2}C_A\alpha_s(1/r) \ll 1$, which holds at sufficiently small r .

9.3 Derivation of Lagrangian and Feynman rules

There are two methods for constructing the Lagrangian of pNRQCD EFT:

1. List up all the operators which are consistent with the symmetry of the theory.
2. Start from $\langle W[A_\mu] \rangle$ in full QCD; redefine fields as appropriate for this system; perform multipole expansion; supplement operators, which originate from scales above μ_f .

In this lecture we explain the latter method.[§]

To set up the necessary formulation, we express the Wilson loop using a bilocal field. (Note that we expressed the Wilson loop using static fields ψ and χ in Sec. 4.2.) We first introduce a bilocal field $\psi(\vec{x}, \vec{y}; t)$, which is a complex scalar field given as an N by N matrix in the $SU(N)$ color space, and which transforms in the same way as $\psi\chi^\dagger$, namely,

$$\psi(\vec{x}, \vec{y}; t) \sim \psi(t, \vec{x}) \chi^\dagger(t, \vec{y}). \quad (114)$$

Using this bilocal field, we can express the Wilson loop eq. (28) as

$$\begin{aligned} & W[A_\mu] \delta^3(\vec{x}_1 - \vec{x}'_1) \delta^3(\vec{x}_2 - \vec{x}'_2) \\ &= \int \mathcal{D}\psi \mathcal{D}\psi^\dagger \exp \left[i \int dt d^3\vec{x} d^3\vec{y} \mathcal{L}[\psi, \psi^\dagger, A_\mu] \right] \\ & \quad \times \text{Tr} [\psi^\dagger(\vec{x}_1, \vec{x}_2; 0) \phi(\vec{x}_1, \vec{x}_2; 0)] \text{Tr} [\psi(\vec{x}'_1, \vec{x}'_2; T) \phi^\dagger(\vec{x}'_1, \vec{x}'_2; T)], \end{aligned} \quad (115)$$

with

$$\begin{aligned} \mathcal{L}[\psi, \psi^\dagger, A_\mu] &= \text{Tr} [\psi^\dagger(\vec{x}, \vec{y}; t) i D_t \psi(\vec{x}, \vec{y}; t)] \\ &= \text{Tr} [\psi^\dagger(\vec{x}, \vec{y}; t) i \partial_t \psi(\vec{x}, \vec{y}; t) + g \psi^\dagger(\vec{x}, \vec{y}; t) A_0(t, \vec{x}) \psi(\vec{x}, \vec{y}; t) \\ & \quad - g \psi^\dagger(\vec{x}, \vec{y}; t) \psi(\vec{x}, \vec{y}; t) A_0(t, \vec{y})]. \end{aligned} \quad (116)$$

Note that the gauge transformation of the bilocal field is given by

$$\psi(\vec{x}, \vec{y}; t) \rightarrow U(\vec{x}, t) \psi(\vec{x}, \vec{y}; t) U^\dagger(\vec{y}, t), \quad (117)$$

so that the covariant derivative in the above Lagrangian is also a bilocal operator. The expression of the Wilson loop in terms of $\psi(\vec{x}, \vec{y}; t)$ can be justified in a similar manner as in Sec. 4.2, by examining the time evolution of the Wilson loop in terms of a differential equation.

We decompose the bilocal field into the singlet and octet components as

$$\psi(\vec{x}, \vec{y}; t) = \phi(\vec{x}, \vec{y}; t) S(\vec{X}, \vec{r}; t) + \phi(\vec{x}, \vec{X}; t) O(\vec{X}, \vec{r}; t) \phi(\vec{X}, \vec{y}; t), \quad (118)$$

[§] This is a simplified version of a more solid method based on the asymptotic expansion (integration by regions) of Feynman diagrams; see Appendix C.

where S is proportional to the identity matrix and O is traceless. Hence, the gauge transformations of these fields are given by

$$S(\vec{X}, \vec{r}; t) \rightarrow S(\vec{X}, \vec{r}; t), \quad (119)$$

$$O(\vec{X}, \vec{r}; t) \rightarrow U(\vec{X}, t) O(\vec{X}, \vec{r}; t) U^\dagger(\vec{X}, t). \quad (120)$$

The singlet and octet fields are defined such that their gauge transformations depend only on \vec{X} and not on \vec{r} . In this way, we can maintain gauge invariance of the theory explicitly at each order of multipole expansion in \vec{r} . (Otherwise different orders of expansion in \vec{r} mix under gauge transformation.) This helps greatly to simplify the interactions of the EFT.

Let us expand $\mathcal{L}[\psi, \psi^\dagger, A_\mu]$ in \vec{r} . The expansion of the color string can be computed as

$$\begin{aligned} \phi(\vec{x}, \vec{y}; t) &= \text{P exp} \left[ig \int_{-1/2}^{1/2} ds \vec{r} \cdot \vec{A}(t, \vec{X} + s\vec{r}) \right] \\ &= \mathbf{1} + ig \int_{-1/2}^{1/2} ds \vec{r} \cdot \vec{A}(t, \vec{X} + s\vec{r}) + \mathcal{O}(r^2) \\ &= \mathbf{1} + ig \vec{r} \cdot \vec{A}(t, \vec{X}) + \mathcal{O}(r^2). \end{aligned} \quad (121)$$

Similarly, we obtain

$$\phi(\vec{x}, \vec{X}; t) = \mathbf{1} + \frac{1}{2} ig \vec{r} \cdot \vec{A}(t, \vec{X}) + \mathcal{O}(r^2), \quad (122)$$

$$\phi(\vec{X}, \vec{y}; t) = \mathbf{1} + \frac{1}{2} ig \vec{r} \cdot \vec{A}(t, \vec{X}) + \mathcal{O}(r^2). \quad (123)$$

We may then express ψ by S and O in expansion in \vec{r} :

$$\begin{aligned} \psi(\vec{x}, \vec{y}; t) &= S(\vec{X}, \vec{r}; t) + ig \vec{r} \cdot \vec{A}(t, \vec{X}) S(\vec{X}, \vec{r}; t) \\ &\quad + O(\vec{X}, \vec{r}; t) + \frac{1}{2} ig \left\{ \vec{r} \cdot \vec{A}(t, \vec{X}), O(\vec{X}, \vec{r}; t) \right\} + \mathcal{O}(r^2). \end{aligned} \quad (124)$$

By substituting this to \mathcal{L} and expanding in \vec{r} , we obtain the following interaction terms up to $\mathcal{O}(r)$:

$$\mathcal{L}_{OS} = g \text{Tr} \left[O^\dagger \vec{r} \cdot \vec{E} S \right] + g \text{Tr} \left[O \vec{r} \cdot \vec{E} S^\dagger \right], \quad (125)$$

$$\mathcal{L}_{SS} = \text{Tr} \left[S^\dagger i \partial_t S \right], \quad (126)$$

$$\mathcal{L}_{OO} = \text{Tr} \left[O^\dagger i D_t O \right] + \frac{1}{2} g \text{Tr} \left[O^\dagger O \vec{r} \cdot \vec{E} \right] + \frac{1}{2} g \text{Tr} \left[O O^\dagger \vec{r} \cdot \vec{E} \right], \quad (127)$$

where $\vec{E} = -\partial_t \vec{A} - \vec{\partial} A_0 - ig[A_0, \vec{A}]$ represents the color electric field. All the gauge fields are evaluated at (t, \vec{X}) .

We should add to the above interactions the ‘‘potential terms’’

$$\mathcal{L}_{\text{pot}} = -\text{Tr} \left[S^\dagger V_S(r) S + O^\dagger V_O(r) O \right], \quad (128)$$

where $V_S(r)$ and $V_O(r)$ represent the singlet and octet potentials, respectively. If we evaluate them in expansions in α_s , the leading terms are given by Coulomb potentials; see eqs. (108) and (109). These arise as contributions from scales above μ_f , from the one-gluon exchange diagram shown left with $E_g > \mu_f$. Intuitively, the singular behaviors as $r \rightarrow 0$ cannot arise from IR gluons whose wavelengths are larger than r , but arise from UV gluons whose wavelengths are smaller than r . In practice, we identify

\mathcal{L}_{pot} by matching to full QCD or by using the integration-by-regions method.

Collecting all the terms, we find

$$\begin{aligned} \mathcal{L} = & \text{Tr} \left[S^\dagger \{i\partial_t - V_S(r)\} S + O^\dagger \{iD_t - V_O(r)\} O \right. \\ & + g S^\dagger O \vec{r} \cdot \vec{E} + g O^\dagger \vec{r} \cdot \vec{E} S + \frac{1}{2} g O^\dagger O \vec{r} \cdot \vec{E} + \frac{1}{2} g O O^\dagger \vec{r} \cdot \vec{E} \left. \right] \\ & + \mathcal{O}(r^2), \end{aligned} \quad (129)$$

Note that $d^3\vec{x} d^3\vec{y} = d^3\vec{X} d^3\vec{r}$ and $\delta^3(\vec{x}) \delta^3(\vec{y}) = \delta^3(\vec{X}) \delta^3(\vec{r})$. As stated, the interactions are gauge invariant at each order of r , and the leading interaction of S and gauge field is of dipole type $\sim g S^\dagger O^a \vec{r} \cdot \vec{E}^a$.

Feynman rules of pNRQCD can be obtained in a straightforward manner from the above Lagrangian. These are given as follows.

Propagators

$$\begin{aligned} & e^{-iV_S(r)(t-t')} \theta(t-t') \delta^3(\vec{r}-\vec{r}') \delta^3(\vec{X}-\vec{X}') \\ & e^{-iV_O(r)(t-t')} [\varphi_{\text{adj}}(t, t')]^{ab} \theta(t-t') \delta^3(\vec{r}-\vec{r}') \delta^3(\vec{X}-\vec{X}') \end{aligned}$$

Vertices

$$\begin{aligned}
 & ig \sqrt{\frac{T_F}{N}} \vec{r} \cdot \vec{E}^b \delta^{ab} \\
 & \frac{1}{2} ig d^{abc} \vec{r} \cdot \vec{E}^c
 \end{aligned}$$

Here, $T_F = \frac{1}{2}$ denotes the trace normalization in the fundamental representation; $d^{abc} = 2\text{Tr}(\{T_F^a, T_F^b\}T_F^c)$ denotes the symmetric invariant tensor; color string for the adjoint representation is given by $\varphi_{\text{adj}}(t, t') = \text{T exp} \left[ig \int_{t'}^t d\tau A_0^c(\tau, \vec{X}) T_{\text{adj}}^c \right]$.

9.4 Computation of $V_{\text{QCD}}(r)$ in pNRQCD

Using the expression of the Wilson loop and Feynman rules derived above, we can compute the expectation value of the Wilson loop in expansion in \vec{r} :

$$\begin{aligned}
 & \langle W[A_\mu] \rangle \delta^3(\vec{X} - \vec{X}') \delta^3(\vec{r} - \vec{r}') \\
 & = \text{Tr} \langle 0 | S(\vec{X}, \vec{r}; T) S^\dagger(\vec{X}', \vec{r}'; 0) | 0 \rangle + \mathcal{O}(r^3) \\
 & = N e^{-iV_S(r)T} \delta^3(\vec{X} - \vec{X}') \delta^3(\vec{r} - \vec{r}') \\
 & \quad \times \left[\mathbf{1} - g^2 \frac{T_F}{N} \int_0^T dt \int_0^t dt' e^{-i(V_O - V_S)(t-t')} \right. \\
 & \quad \left. \times \langle 0 | \vec{r} \cdot \vec{E}^a(t, \vec{X}) [\varphi_{\text{adj}}(t, t')]^{ab} \vec{r} \cdot \vec{E}^b(t', \vec{X}) | 0 \rangle \right] + \mathcal{O}(r^3), \quad (130)
 \end{aligned}$$

where $N = 3$ for QCD. The order r^0 and r^2 terms in the last line correspond to the diagrams below.



On the other hand, in full QCD, we have

$$\langle W[A_\mu] \rangle = \text{const.} \times e^{-iV_{\text{QCD}}(r)T} \quad \text{as} \quad T \rightarrow \infty. \quad (131)$$

Hence, by equating both quantities, we obtain the matching relation of the static potential as

$$V_{\text{QCD}}(r) = V_S(r) - ig^2 \frac{T_F}{N} \int_0^\infty dt e^{-i(V_O - V_S)t} \langle \vec{r} \cdot \vec{E}^a(t, \vec{0}) \varphi_{\text{adj}}(t, 0)^{ab} \vec{r} \cdot \vec{E}^b(0, \vec{0}) \rangle + \mathcal{O}(r^3). \quad (132)$$

Note that, in deriving this relation, we only used expansion in \vec{r} but did not use expansion in α_s .

Let us call the second term of eq. (132) as $V_{\text{IR}}(r)$ and proceed with computation of this quantity, using expansion in α_s and in dimensional regularization. (Expansion in α_s makes sense only in the case that the relevant scale of V_{IR} is much larger than Λ_{QCD} scale, but here we are more interested in the formal structure of V_{IR} in α_s expansion.) Since $\varphi_{\text{adj}}(t, 0)^{ab} = \delta^{ab} + \mathcal{O}(\alpha_s)$, we drop the $\mathcal{O}(\alpha_s)$ term and compute

$$V_{\text{IR}}(r) \approx -ig^2 \frac{T_F}{N} \int_0^\infty dt e^{-it\Delta V(r)} \langle \vec{r} \cdot \vec{E}^a(t) \vec{r} \cdot \vec{E}^a(0) \rangle; \quad \Delta V = V_O - V_S. \quad (133)$$

The following formulas can be used for the computation:

$$\langle \vec{r} \cdot \vec{E}^a(t) \vec{r} \cdot \vec{E}^a(0) \rangle = \frac{r^2}{d} \langle \vec{E}^a(t) \cdot \vec{E}^a(0) \rangle, \quad (134)$$

$$\begin{aligned} \langle E^{ia}(x) E^{ja}(y) \rangle &= \delta^{aa} \langle (\partial^0 A^i(x) - \partial^i A^0(x)) (\partial^0 A^j(y) - \partial^j A^0(y)) \rangle + \mathcal{O}(\alpha_s) \\ &= -i \frac{C_F C_A}{T_F} \int \frac{d^D k}{(2\pi)^D} \frac{e^{ik \cdot (x-y)}}{k^2 + i0} [k^i k^j - (k_0)^2 \delta^{ij}] + \mathcal{O}(\alpha_s), \end{aligned} \quad (135)$$

where $d = D - 1 = 3 - 2\epsilon$ represents the dimensions of space. Integrating over k_0 , we obtain

$$\begin{aligned} \langle \vec{E}^a(t) \cdot \vec{E}^a(0) \rangle &\approx -i \frac{C_F C_A}{T_F} \int \frac{d^D k}{(2\pi)^D} \frac{e^{ik_0 t}}{k^2 + i0} (\vec{k}^2 - d \cdot k_0^2) \\ &= -\frac{C_F C_A}{T_F} \left[\frac{1-d}{2} \int \frac{d^d \vec{k}}{(2\pi)^d} |\vec{k}| e^{-i|\vec{k}|t} - id \cdot \delta(t) \int \frac{d^d \vec{k}}{(2\pi)^d} 1 \right]. \end{aligned} \quad (136)$$

In dimensional regularization the second term vanishes, since it is proportional to a scaleless integral. Hence, we find

$$V_{\text{IR}}(r) \approx -4\pi\alpha_s \bar{\mu}^{2\epsilon} \frac{d-1}{2d} C_F r^2 \int \frac{d^d \vec{k}}{(2\pi)^d} \frac{k}{k + \Delta V}; \quad k = |\vec{k}|, \quad (137)$$

cf. eqs. (10) and (12). This has a form, which we anticipated in Sec. 9.1.

9.5 Matching to QCD

Let us first examine a matching to full QCD in naive expansion in α_s . Namely, we expand the integrand of eq. (137) in α_s before integrating over \vec{k} . If we do so, the integral vanishes, since $\Delta V \approx \frac{C_A}{2} \frac{\alpha_s}{r}$ [c.f., eq. (110)], and

$$\int \frac{d^d \vec{k}}{(2\pi)^d} k^P = 0 \quad (138)$$

for an integer P . (Scaleless integrals vanish in dimensional regularization.) In fact, the second term of the matching relation (132) [$V_{\text{IR}}(r)$] vanishes to all orders in α_s , if we expand it in α_s before integration, since only scaleless integrals appear. Consequently, we find that $V_S(r)$ coincides with the naive expansion of $V_{\text{QCD}}(r)$ in α_s :

$$V_S(r) = V_{\text{QCD}}(r) \Big|_{\text{exp. in } \alpha_s}. \quad (139)$$

Next we perform a matching consistent with the concept of pNRQCD, which we explained in Sec. 9.2. There, we have specified the expansion parameters of the EFT. In particular, since $E_g \lesssim \Delta V$, we should not expand the integrand of eq. (137) by ΔV . If we perform the integration of eq. (137) as it is, it contains a UV divergence and is evaluated to be[¶]

$$\begin{aligned} V_{\text{IR}}(r) &\approx \frac{C_F \alpha_s}{\pi} \frac{r^2}{3} \Delta V^3 \left[\frac{1}{\epsilon} - \gamma_E - \log\left(\frac{\Delta V^2}{\pi \bar{\mu}^2}\right) + \frac{5}{3} \right] \\ &\approx \frac{C_F C_A^3 \alpha_s^4}{24\pi r} \left[\frac{1}{\epsilon} + 8 \log(\bar{\mu} r) - 2 \log(C_A \alpha_s) + \frac{5}{3} + 6\gamma_E \right]. \end{aligned} \quad (142)$$

At this stage we list some known facts concerning this result and the matching relation (132).

- (I) On the right-hand side of eq. (132), the following two contributions cancel: (1) the IR divergence $\sim \frac{\alpha_s^4}{r} \times \frac{1}{\epsilon}$ contained in the first term $V_S(r)$ [= α_s -expansion of $V_{\text{QCD}}(r)$] at three loop, and (2) the UV divergence $\sim \alpha_s r^2 \Delta V^3 \frac{1}{\epsilon}$ contained in the second term $V_{\text{IR}}(r)$ [eq. (142)].

[¶] One can use a formula

$$\int \frac{d^d \vec{k}}{(2\pi)^d} \frac{k^n}{(k+a)^\nu} = 2^{1-d} \pi^{-\nu/2} \frac{\Gamma(n+d)\Gamma(\nu-n-d)}{\Gamma(d/2)\Gamma(\nu)} a^{d+n-\nu} \quad (140)$$

to evaluate the integral. Note that

$$\Delta V = \frac{C_A}{2} \frac{\alpha_s}{r} (\bar{\mu} r)^{2\epsilon} \frac{\Gamma(\frac{1}{2}-\epsilon)}{\pi^{\frac{1}{2}-\epsilon}} + O(\alpha_s^2) \quad (141)$$

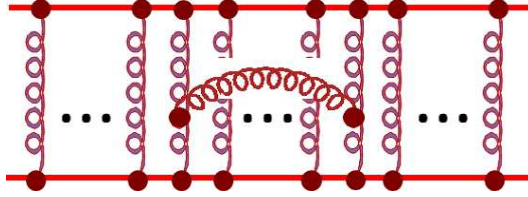
in dimensional regularization.

(II) The right-hand side of eq. (132) altogether is finite as $\epsilon \rightarrow 0$ and includes

$$C_F \alpha_s r^2 \Delta V^3 \log(r^2 \Delta V^2) \sim \frac{C_F C_A^3 \alpha_s^4}{r} \log(C_A^2 \alpha_s^2).$$

[Compare the argument on collinear divergence and $\log(E_e/m_e)$ in Sec. 9.1.]

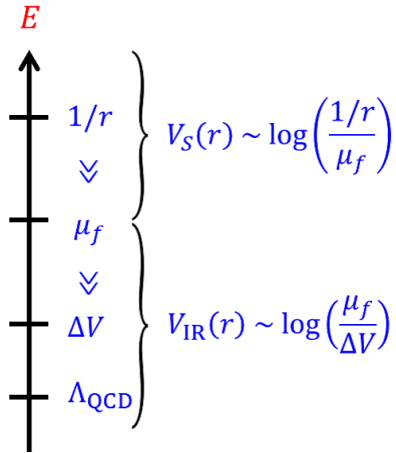
(III) The right-hand side of eq. (132) altogether coincides with the resummation of ladder-type diagrams for $V_{\text{QCD}}(r)$ shown below, which was suggested by Appelquist, Dine and Muzunich to remedy apparent IR divergences of $V_{\text{QCD}}(r)$.



(IV) $V_{\text{QCD}}(r)$ can be computed systematically in double expansion in α_s and $\log \alpha_s$ using pNRQCD.

9.6 Renormalization of Wilson coefficient and μ_f -independence of $V_{\text{QCD}}(r)$

The IR divergence of the (bare) Wilson coefficient $V_S(r)$ and the UV divergence of $V_{\text{IR}}(r)$ in pNRQCD are considered as artifacts of dimensional regularization without a cutoff



in momentum space. Had we integrated out energy scales above the factorization scale μ_f à la Wilson, $V_S(r)$ would have contained $\log(r^{-1}/\mu_f)$ and $V_{\text{IR}}(r)$ would have contained $\log(\mu_f/\Delta V)$ in such a way that μ_f dependences cancel in the sum. Physically we expect to replace the pole in ϵ corresponding to the IR divergence of $V_S(r)$ by $\log(r^{-1}/\mu_f)$, while we expect to replace the pole corresponding to the UV divergence in $V_{\text{IR}}(r)$ by $\log(\mu_f/\Delta V)$.^{*} This is the renormalization in pNRQCD. Thus, the cancellation of $1/\epsilon$'s in $V_S(r)$ and $V_{\text{IR}}(r)$ implies cancellation of μ_f -dependences, which follows from the fact that $V_{\text{QCD}}(r)$ should not depend on how to factorize the energy scale.

The renormalization of $V_S(r)$ and $V_{\text{IR}}(r)$ is not important as long as we are interested in evaluating their sum in double expansion in α_s and $\log \alpha_s$, since the sum does not

^{*} For instance, one may compare with the chiral perturbation theory formulated in dimensional regularization, in which UV divergences represented by poles in ϵ are interpreted as logarithms of cut-off scale $\sim \log(4\pi f_\pi)$.

depend on the renormalization scheme if expressed by the parameters of full QCD (perturbative QCD). The renormalization becomes important in the case that we evaluate $V_{\text{IR}}(r)$ non-perturbatively, such as by using lattice computations, while $V_S(r)$ is evaluated perturbatively. In particular it becomes quite important to subtract the IR renormalons contained in $V_S(r)$ in the case that we use dimensional regularization.

Due to technical simplicity, $V_S(r)$ is often computed in dimensional regularization using the relation (139). Elimination of IR contributions from $V_S(r)$ is not automatic in this case, unlike the case where we explicitly introduce a cut-off (corresponding to the factorization scale μ_f) in the computation. Indeed the bare $V_S(r)$ in dimensional regularization [= naive expansion of $V_{\text{QCD}}(r)$ in α_s] contains IR renormalons just as we explained in Sec. 5. The $\mathcal{O}(\Lambda_{\text{QCD}}^3 r^2)$ renormalon should be subtracted from $V_S(r)$. It is absorbed in or replaced by a non-perturbative matrix element in $V_{\text{IR}}(r)$.[†] Otherwise one would inflate uncertainties in the perturbative prediction of $V_S(r)$ as an artifact of dimensional regularization. We present specific renormalization schemes of Wilson coefficients below.

9.7 Renormalons in $V_{\text{IR}}(r)$

As it is clear from its construction, pNRQCD EFT reproduces correctly the dynamics of QCD in the IR region relevant to the static $Q\bar{Q}$ system. Therefore, the $\mathcal{O}(\Lambda_{\text{QCD}}^3 r^2)$ IR renormalon of $V_{\text{QCD}}(r)$, which we analyzed in Sec. 6, should be reproduced in $V_{\text{IR}}(r)$. Due to the relation (139) and the argument in the previous subsection, the $\mathcal{O}(\Lambda_{\text{QCD}}^3 r^2)$ IR renormalon should arise from the region $k \gg \Delta V$ in $V_{\text{IR}}(r)$. Namely, the region is IR compared to the scale $1/r$, but we did not take account of the scale ΔV in Sec. 6, which is invisible in naive expansion in α_s .

Let us check this statement by introducing a cut-off in the gluon momentum instead of dimensional regularization in eq. (136). In this case, the second term of eq. (136) cannot be dropped. Integration of $\delta(t)$ over the range $t \geq 0$ has a subtlety, and we find that the proper prescription is to set this equal to $1/2$.[‡] Hence, by comparing to eq. (137), one finds

$$\begin{aligned}
& [\mathcal{O}(\Lambda_{\text{QCD}}^3 r^2) \text{ renormalon of } V_{\text{IR}}(r)] \\
& \sim -4\pi\alpha_s \cdot \frac{2}{6} \cdot C_F r^2 \int_{k < \mu_f} \frac{d^3 \vec{k}}{(2\pi)^3} \left[\frac{k}{k + \Delta V} - \frac{3}{2} \right]_{k \gg \Delta V} \\
& \sim \int_{k < \mu_f} \frac{d^3 \vec{k}}{(2\pi)^3} \left[-C_F \frac{4\pi\alpha_s}{k^2} \right] \cdot \frac{1}{2} (i\vec{k} \cdot \vec{r})^2, \tag{143}
\end{aligned}$$

[†] Here and hereafter, we are mainly interested in the $\mathcal{O}(\Lambda_{\text{QCD}}^3 r^2)$ renormalon and ignore the $\mathcal{O}(\Lambda_{\text{QCD}})$ renormalon which can be canceled against that of $2m_{\text{pole}}$ in the total energy.

[‡] It is always possible to clarify the proper prescription, since one can check equivalence of pNRQCD with full QCD in IR region at every stage of deriving Feynman rules.

where we used the fact that the angular average of $k^i k^j / k^2$ is equal to $\delta^{ij}/3$. If we resum LLs, we can check that, in the region $\Delta V \ll k < \mu_f$, the coupling constant α_s of eq. (143) is replaced by the one-loop running coupling constant $\alpha_{\text{1L}}(k)$. Thus, indeed it has the same form as the $\mathcal{O}(\Lambda_{\text{QCD}}^3 r^2)$ renormalon which we analyzed in Sec. 6.2. Simultaneously this also shows that the μ_f -dependences of the r^2 terms cancel in eq. (99), as we claimed.[§]

The above analysis suggests certain renormalization schemes for $V_S(r)$ and $V_{\text{IR}}(r)$, which we discussed in the previous subsection. We can convert IR contributions to $V_{\text{QCD}}(r)$ from dimensional regularization to a cut-off regularization, which matches the purpose of the renormalization. By taking the difference of $V_{\text{IR}}(r)$ [eq. (133)] in dimensional regularization and in a cut-off regularization, we obtain the counter term as

$$\begin{aligned} [\delta_{c.t.} V_S(r)]_{\text{cut-off}} &= [\text{eq. (142)}] - \left[-\frac{4\pi\alpha_s}{3} \cdot C_F r^2 \int_{k < \mu_f} \frac{d^3 \vec{k}}{(2\pi)^3} \left(\frac{k}{k + \Delta V} - \frac{3}{2} \right) \right] \\ &= \frac{C_F \alpha_s}{9\pi r} \left[-(\mu_f r)^3 - \frac{3}{2} C_A \alpha_s \cdot (\mu_f r)^2 + \frac{3}{2} C_A^2 \alpha_s^2 \cdot (\mu_f r) \right. \\ &\quad \left. + C_A^3 \alpha_s^3 \left\{ \frac{3}{4} \log \left(\frac{\mu^4 r^3}{2\mu_f} \right) + \frac{3}{8\epsilon} + \frac{9}{4} \gamma_E + \frac{5}{8} \right\} \right], \end{aligned} \quad (144)$$

which should be added to $V_S(r)$ in dimensional regularization [bare $V_S(r)$]. We see a strong dependence on the factorization scale $\sim \mu_f^3 r^2$ reflecting the cubic divergence of the \vec{k} integration.

The above renormalization scheme may not be optimal, since generally a cut-off in gluon momenta introduces gauge dependences. Another sensible renormalization scheme is to subtract only the IR renormalon and IR divergences from the bare $V_S(r)$, since they cause the main (known) problems of the perturbative series and can be extracted in a gauge-independent manner. For instance, we can add the sum of the following two counter terms, which are derived from an estimate similar to eq. (79) for the $\mathcal{O}(\Lambda_{\text{QCD}}^3 r^2)$ renormalon and $\overline{\text{MS}}$ renormalization of IR divergence, respectively:

$$[\delta_{c.t.} V_S(r)]_{\text{renormalons}} = -\frac{C_F \alpha_s}{9\pi} (\mu e^{5/6})^3 r^2 \sum_{n=0}^{\infty} \left(\frac{\beta_0 \alpha_s}{4\pi} \cdot \frac{2}{3} \right)^n n!, \quad (145)$$

$$[\delta_{c.t.} \tilde{V}_S(q)]_{\text{IR-div.}} = \frac{C_F C_A^3 \alpha_s^4}{6q^2} \frac{1}{\epsilon} + \mathcal{O}(\alpha_s^5), \quad (146)$$

[§] Note that, since $\mu_f \gg \Lambda_{\text{QCD}}$, μ_f -dependence of V_{IR} can be estimated reliably in expansion in α_s , even in the case that a dominant part of V_{IR} is non-perturbative.

where the counter term in the $\overline{\text{MS}}$ scheme is added in momentum space.[¶]

Using the result of Sec. 7.2, we may define an alternative renormalization scheme as follows. We define the renormalized $V_S(r)$ as

$$[V_S(r)]_{\text{ren}} = V_C(r) + \sigma r, \quad (148)$$

where

$$V_C(r) = \frac{A}{r} - \frac{2C_F}{\pi} \text{Im} \int_{C_1} dq \frac{e^{iqr}}{qr} \alpha_{1L}(q), \quad (149)$$

$$A = -\frac{C_F}{\pi i} \int_{C_2} dq \frac{\alpha_{1L}(q)}{qr}, \quad \sigma = \frac{C_F}{2\pi i} \int_{C_2} dq q \alpha_{1L}(q), \quad (150)$$

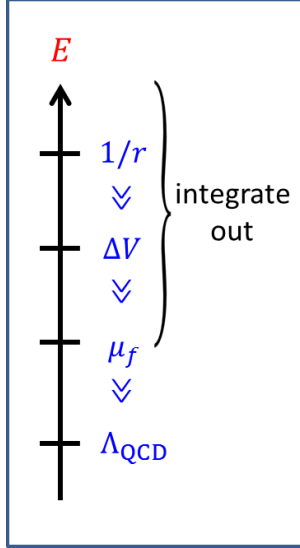
in the LL approximation. This formula subtracts IR contributions by resummation of logarithms and contour integral surrounding the singularity at $q = \Lambda_{\text{QCD}}$. The formula can be extended naturally to include subleading logarithms. In this case the running coupling constant can be determined from perturbative evaluation of $V_S(r)$ in momentum space, $\tilde{V}_S(q)$, after resummation of logarithms by RG equation. From NNNLL the bare $\tilde{V}_S(q)$ includes IR divergences originating from the scale $\Delta V \ll k \ll 1/r$. The contour deformation subtracts the $\mathcal{O}(\Lambda_{\text{QCD}}^3 r^2)$ renormalon but not the IR divergences which stem from deeper loop levels. We subtract the IR divergences in the $\overline{\text{MS}}$ scheme.

By making the scale ΔV explicit, an IR structure of $V_{\text{QCD}}(r)$ concealed in the naive perturbative expansion has become visible. Eq. (143) shows that the IR behavior of $V_{\text{IR}}(r)$ is different from the IR behavior of $V_S(r)$. From the behavior of $V_{\text{IR}}(r)$ at $k \sim 0$, one can estimate that it contains an $\mathcal{O}(\Lambda_{\text{QCD}}^4 r^3)$ IR renormalon. This means that, if $V_{\text{IR}}(r)$ is examined in a double expansion in α_s and $\log \alpha_s$, it contains an $\mathcal{O}(\Lambda_{\text{QCD}}^4 r^3)$ IR renormalon. This leads to an interesting consequence. We found in Sec. 6 that the leading IR renormalon of $E_{\text{tot}}(r)$ is $\mathcal{O}(\Lambda_{\text{QCD}}^3 r^2)$. In other words, the leading IR renormalon of $2m_{\text{pole}} + V_S(r)$ for the bare $V_S(r)$ is $\mathcal{O}(\Lambda_{\text{QCD}}^3 r^2)$. In contrast, the leading IR renormalon of $2m_{\text{pole}} + V_S(r) + V_{\text{IR}}(r)$ is $\mathcal{O}(\Lambda_{\text{QCD}}^4 r^3)$ if it is examined in a double expansion in α_s and $\log \alpha_s$. Thus, the renormalon uncertainty of the perturbative series for the total energy of the $Q\bar{Q}$ system at small r ($\ll \Lambda_{\text{QCD}}^{-1}$) can be reduced step by step.

[¶] The relation between the potentials in coordinate space and momentum space is given by

$$V_S(r) = \bar{\mu}^{2\epsilon} \int \frac{d^d \vec{q}}{(2\pi)^d} e^{i\vec{q}\cdot\vec{r}} \tilde{V}_S(q). \quad (147)$$

9.8 $V_{\text{QCD}}(r)$ at very small r and local gluon condensate^{||}



At very short distances $r \rightarrow 0$, we can assume $\Delta V(r) \sim 1/|r \log(\Lambda_{\text{QCD}} r)| \gg \Lambda_{\text{QCD}}$. Then it is possible to choose the factorization scale as $\Lambda_{\text{QCD}} \ll \mu_f \ll \Delta V$ and integrate out all the scales above μ_f . In this case, only the scale Λ_{QCD} remains as dynamical degrees of freedom. Such an EFT describes dynamics of gluons with energies $E_g \sim \Lambda_{\text{QCD}} \ll \Delta V$, which interact with the $Q\bar{Q}$ system. The fields of the EFT are S , O and A_μ , the same as those of pNRQCD. In addition to the expansion parameters of pNRQCD, we have $E_g/\Delta V \ll 1$. Hence, we can regard ∂_t operating on A_μ to be small.

The matching relation (132) changes to

$$V_{\text{QCD}}(r) = V_S(r) + V_{\text{IR}}(r) - ig^2 \frac{T_F}{N} \int_0^\infty dt e^{-it\Delta V} \left[\langle \vec{r} \cdot \vec{E}^a(0, \vec{0}) \vec{r} \cdot \vec{E}^a(0, \vec{0}) \rangle + \mathcal{O}(t) \right] + \mathcal{O}(r^3) \quad (151)$$

in this EFT. We have expanded the matrix element in t ; if we transform the integral variable to $\tau = t\Delta V$, it is easy to see that this expansion generates essentially an expansion in $E_g/\Delta V$. In this EFT, the energy region $E \sim \Delta V \gg \Lambda_{\text{QCD}}$ is included in Wilson coefficients. Thus, perturbative evaluation of V_{IR} , given by eq. (142), is treated as a UV contribution. Note that the above matching relation is consistent both in naive expansion in α_s ($V_{\text{IR}} = 0$ in this case) and in double expansion in α_s and $\log \alpha_s$ in dimensional regularization; in both cases the third term evaluates to zero, since it is given by scaleless integrals.

Noting that

$$\langle 0 | G_{\mu\nu}^a(0) G_{\rho\sigma}^a(0) | 0 \rangle \propto g_{\mu\rho} g_{\nu\sigma} - g_{\nu\rho} g_{\mu\sigma} \quad (152)$$

by antisymmetry of $G_{\mu\nu}^a$ and Lorentz invariance of the vacuum, it follows that

$$\langle 0 | G^{\mu\nu a}(0) G_{\mu\nu}^a(0) | 0 \rangle = -D \langle 0 | \vec{E}^a(0) \cdot \vec{E}^a(0) | 0 \rangle. \quad (153)$$

Hence, the leading non-perturbative contribution in eq. (151) can be expressed by the local gluon condensate (Voloshin, Leutwelyer):

$$\frac{T_F}{ND(D-1)} \frac{r^2}{\Delta V} \langle 0 | g^2 G^{\mu\nu a}(0) G_{\mu\nu}^a(0) | 0 \rangle. \quad (154)$$

This shows that the non-perturbative contribution is given by $\sim \Lambda_{\text{QCD}}^4 r^3$ at very short distances. In fact, it follows from a purely dimensional analysis, since there is no other

^{||} The contents of this subsection are still premature and many properties are yet to be tested quantitatively.

scale than Λ_{QCD} and the lowest-dimensional local operator of the gauge field is the local gluon condensate $\sim \Lambda_{\text{QCD}}^4$. We also note that this matches the IR renormalon of V_{IR} discussed in the previous section.

The bare $V_S(r) + V_{\text{IR}}(r)$ (which is evaluated in double expansion in α_s and $\log \alpha_s$ in dimensional regularization) is free from IR divergences, as stated at the end of Sec. 9.5. Nevertheless, it contains IR renormalons, and in general all the IR contributions (including the renormalons) should be subtracted by renormalization. Noting that the non-perturbative contribution (154) is zero in double expansion in α_s and $\log \alpha_s$, and according to the interpretation which we explained below eq. (99), it is legitimate to define the renormalized $V_S(r) + V_{\text{IR}}(r)$ in the following way:

$$[V_S(r) + V_{\text{IR}}(r)]_{\text{ren}} = V_C(r) + \sigma r, \quad (155)$$

where, in this case, the running coupling constant is determined from perturbative evaluation of $V_S(r) + V_{\text{IR}}(r)$ in momentum space, after resummation of logarithms by RG equation. It is free of IR divergences and includes contributions from scales $E \sim \Delta V$ and higher. By contour deformation method, contributions only from the scale Λ_{QCD} are subtracted from it. This definition is consistent with the fact that the residual non-perturbative contributions include only the scale Λ_{QCD} . Note that, up to NNLL, the perturbative evaluation of V_{IR} in dimensional regularization vanishes, so that there is no distinction whether the scale ΔV is included in $V_C(r) + \sigma r$ or not up to this order.

To end Sec. 9, let us make some remarks. As we have seen, pNRQCD (in the static limit) provides a powerful tool to analyze IR dynamics of the heavy $Q\bar{Q}$ states systematically using multipole expansion. It clarifies how to factorize IR contributions. In this way, perturbative predictions of UV contributions can be made accurate, free from IR divergences and IR renormalons, by replacing IR contributions by non-perturbative matrix elements.

Nevertheless, at the present status, we find that the following question needs to be understood better. In principle, IR contributions in perturbative computations can be defined unambiguously if we introduce a cut-off in gluon momenta, which is close to the original idea of Wilson. This introduces, however, gauge dependence and perhaps artificially strong dependences on the cut-off μ_f . Hence, it is desirable to find more sophisticated ways to subtract IR contributions from Wilson coefficients. We have suggested two ways in this lecture: (i) to subtract IR divergences and estimates of IR renormalons, and (ii) to subtract IR contribution as a contour integral surrounding a singularity after resummations of logarithms. In either method, one needs to understand the structure of IR renormalons in advance. In detailed analyses which go beyond the LL level, one finds different types of IR renormalons by inspection of certain series of higher-order terms of perturbative expansion. It is quite challenging to identify them exhaustively or organize them systematically. We would like to study further to which extent this is possible. The correspondence between the renormalons and non-perturbative matrix elements of EFT would play a key role in such an analysis.

10 References for Further Studies

In this section we list some references which are useful for further studies.

Sec. 2

For reviews of semi-quantitative descriptions of the dynamics of chiral symmetry breaking in QCD using Nambu-Jona-Lasino model and Schwinger-Dyson equation, see:

- 2-1. K. Higashijima, “Dynamical Chiral Symmetry Breaking,” *Phys. Rev. D* **29** (1984) 1228; K. Higashijima, “Theory of dynamical symmetry breaking,” *Prog. Theor. Phys. Suppl.* **104** (1991) 1.
- 2-2. K. I. Aoki, M. Bando, T. Kugo, M. G. Mitchard and H. Nakatani, “Calculating the decay constant F_π ,” *Prog. Theor. Phys.* **84** (1990) 683.

Sec. 3

There are many good textbooks and reviews on renormalization and renormalization-group equation in QCD. See, for example:

- 3-1. J. C. Collins, “Renormalization — *An introduction to renormalization, the renormalization group, and the operator-product expansion*,” Cambridge University Press, (1986), ISBN: 9780521311779.
- 3-2. D. J. Gross, “Applications of the Renormalization Group to High-Energy Physics,” in *Les Houches 1975, Proceedings, Methods In Field Theory*, Amsterdam 1976, p.141–250.

Sec. 4

For a connection between the static QCD potential and the heavy quark effective theory, see, for example:

- 4-1. M. Peter, “The Static potential in QCD: A Full two loop calculation,” *Nucl. Phys. B* **501** (1997) 471 [hep-ph/9702245].

A review on the lattice computations of the static QCD potential in maximally abelian gauge and connection with dual-Meissner effects can be found in:

- 4-2. H. Ichie, “Dual Higgs theory for color confinement in quantum chromodynamics,” hep-lat/9906005.

Sec. 5

Reviews on large-order behaviors of perturbative series and asymptotic series can be found in:

- 5-1. J. C. Le Guillou and J. Zinn-Justin, “Large order behavior of perturbation theory,” Amsterdam, Netherlands: North-Holland (1990), ISBN: 978-0-444-88597-5.
- 5-2. J. Zinn-Justin, “Perturbation Series at Large Orders in Quantum Mechanics and Field Theories: Application to the Problem of Resummation,” Phys. Rept. **70** (1981) 109.
- 5-3. R. B. Dingle, “Asymptotic Expansions: Their Derivation and Interpretation,” Academic Press, 1973, ISBN-10: 0122165500.

For a review on renormalons, see:

- 5-4. M. Beneke, “Renormalons,” Phys. Rept. **317** (1999) 1 [hep-ph/9807443].

Renormalons in the static potential were first discussed in:

- 5-5. U. Aglietti and Z. Ligeti, “Renormalons and confinement,” Phys. Lett. B **364** (1995) 75 [hep-ph/9503209].

Sec. 6

The cancellation of renormalons in the total energy was discovered by:

- 6-1. A. Pineda, “Heavy Quarkonium and Nonrelativistic Effective Field Theories,” Ph.D. Thesis, <http://www.slac.stanford.edu/spires/find/hep/www?irn=5399084>; A. H. Hoang, M. C. Smith, T. Stelzer and S. Willenbrock, “Quarkonia and the pole mass,” Phys. Rev. D **59**, 114014 (1999) [arXiv:hep-ph/9804227]; M. Beneke, “A quark mass definition adequate for threshold problems,” Phys. Lett. B **434**, 115 (1998) [arXiv:hep-ph/9804241].

Details of the numerical results of the perturbative series in Sec. 6.3 are given in:

- 6-2. Y. Sumino, “A connection between the perturbative QCD potential and phenomenological potentials,” Phys. Rev. D **65**, 054003 (2002) [arXiv:hep-ph/0104259]; S. Recksiegel and Y. Sumino, “Perturbative QCD potential, renormalon cancellation and phenomenological potentials,” Phys. Rev. D **65**, 054018 (2002) [arXiv:hep-ph/0109122].

The three-loop [$\mathcal{O}(\alpha_s^4)$] corrections to the QCD potential were computed in:

- 6-3. A. V. Smirnov, V. A. Smirnov and M. Steinhauser, “Fermionic contributions to the three-loop static potential,” Phys. Lett. B **668**, 293 (2008) [arXiv:0809.1927 [hep-ph]].

- 6-4. C. Anzai, Y. Kiyo and Y. Sumino, “Static QCD potential at three-loop order,” Phys. Rev. Lett. **104**, 112003 (2010) [arXiv:0911.4335 [hep-ph]]; A. V. Smirnov, V. A. Smirnov and M. Steinhauser, “Three-loop static potential,” Phys. Rev. Lett. **104**, 112002 (2010) [arXiv:0911.4742 [hep-ph]].

The relation between the pole and $\overline{\text{MS}}$ masses in the large- β_0 approximation is computed in:

- 6-5. M. Beneke and V. M. Braun, “Naive non-abelianization and resummation of fermion bubble chains,” Phys. Lett. B **348** (1995) 513 [hep-ph/9411229].

A compelling evidence of IR renormalons is presented in:

- 6-6. C. Bauer, G. S. Bali and A. Pineda, “Compelling Evidence of Renormalons in QCD from High Order Perturbative Expansions,” Phys. Rev. Lett. **108** (2012) 242002 [arXiv:1111.3946 [hep-ph]].

Sec. 7

The idea of Wilsonian low-energy EFT is explained fully in:

- 7-1. K. G. Wilson and J. B. Kogut, “The Renormalization group and the epsilon expansion,” Phys. Rept. **12** (1974) 75.

A short-distance expansion of UV contributions to $V_{\text{QCD}}(r)$ and their analytic evaluation can be found in:

- 7-2. Y. Sumino, “Static QCD Potential at $r < \Lambda_{\text{QCD}}^{-1}$: perturbative expansion and operator-product expansion,” Phys. Rev. D **76**, 114009 (2007) [arXiv:hep-ph/0505034].

The method of “integration by regions” to calculate asymptotic expansion of Feynman diagrams is explained in:

- 7-3. V. A. Smirnov, “Applied asymptotic expansions in momenta and masses,” Springer Tracts Mod. Phys. **177** (2002), ISBN-10: 3540423346.
- 7-4. M. Beneke and V. A. Smirnov, “Asymptotic expansion of Feynman integrals near threshold,” Nucl. Phys. B **522** (1998) 321 [hep-ph/9711391].

A justification of this method is given in:

- 7-5. B. Jantzen, “Foundation and generalization of the expansion by regions,” JHEP **1112** (2011) 076 [arXiv:1111.2589 [hep-ph]].

Sec. 8

Microscopic composition of the energy inside the bottomonium states using their wave functions is discussed in:

- 8-1. N. Brambilla, Y. Sumino and A. Vairo, “Quarkonium spectroscopy and perturbative QCD: A New perspective,” *Phys. Lett. B* **513** (2001) 381.
- 8-2. S. Recksiegel and Y. Sumino, “Improved perturbative QCD prediction of the bottomonium spectrum,” *Phys. Rev. D* **67** (2003) 014004 [hep-ph/0207005].

Sec. 9

Potential-NRQCD EFT in the static quark limit is discussed extensively in:

- 9-1. N. Brambilla, A. Pineda, J. Soto and A. Vairo, “Potential NRQCD: An Effective theory for heavy quarkonium,” *Nucl. Phys. B* **566** (2000) 275 [hep-ph/9907240].

The IR divergence of $V_{\text{QCD}}(r)$ from three loops was found by:

- 9-2. T. Appelquist, M. Dine and I. J. Muzinich, “The Static Limit Of Quantum Chromodynamics,” *Phys. Rev. D* **17**, 2074 (1978).

Its full identification within pNRQCD was given in Ref.[9-1] and

- 9-3. B. A. Kniehl and A. A. Penin, “Ultrasoft effects in heavy quarkonium physics,” *Nucl. Phys. B* **563**, 200 (1999).

The facts (I)–(IV) listed at the end of Sec. 9.5 are verified in:

- 9-4. C. Anzai, Y. Kiyo and Y. Sumino, “Violation of Casimir Scaling for Static QCD Potential at Three-loop Order,” *Nucl. Phys. B* **838** (2010) 28 [arXiv:1004.1562 [hep-ph]].

Renormalization of Wilson coefficients in OPE of $V_{\text{QCD}}(r)$ is discussed in:

- 9-5. A. Pineda, “The Static potential: Lattice versus perturbation theory in a renormalon based approach,” *J. Phys. G* **29** (2003) 371 [hep-ph/0208031],

and in Ref.[7-2].

The mechanism how a double expansion in α_s and $\log \alpha_s$ can modify the structure of renormalon from $\mathcal{O}(\Lambda_{\text{QCD}}^3)$ to $\mathcal{O}(\Lambda_{\text{QCD}}^4)$ is discussed in:

- 9-6. Y. Kiyo and Y. Sumino, “Off-shell suppression of renormalons in nonrelativistic QCD bound states,” *Phys. Lett. B* **535** (2002) 145 [hep-ph/0110277].

An analysis of renormalons in $V_{\text{IR}}(r)$ in the large- β_0 approximation and using its Borel transform is given in:

9-7. Y. Sumino, “‘Coulomb + linear’ form of the static QCD potential in operator product expansion,” *Phys. Lett. B* **595** (2004) 387 [hep-ph/0403242].

The non-perturbative correction in terms of local gluon condensate was derived by

9-8. M. B. Voloshin, “On Dynamics of Heavy Quarks in Nonperturbative QCD Vacuum,” *Nucl. Phys. B* **154** (1979) 365; H. Leutwyler, “How to Use Heavy Quarks to Probe the QCD Vacuum,” *Phys. Lett. B* **98** (1981) 447,

and in Ref.[9-1] in the framework of pNRQCD.

Applications

To compute observables of heavy quarkonium states using pNRQCD, it is necessary to go beyond the static limit and include corrections in expansion in $1/m_Q$. For the study in this direction we refer to a review:

A-1. N. Brambilla, A. Pineda, J. Soto and A. Vairo, “Effective field theories for heavy quarkonium,” *Rev. Mod. Phys.* **77** (2005) 1423 [arXiv:hep-ph/0410047].

In particular, the full NNNLO Hamiltonian for the heavy quarkonium was computed in:

A-2. B. A. Kniehl, A. A. Penin, V. A. Smirnov and M. Steinhauser, “Potential NRQCD and heavy quarkonium spectrum at next-to-next-to-next-to-leading order,” *Nucl. Phys. B* **635** (2002) 357,

(completed with the three-loop static potential in Refs.[6-3] and [6-4]).

Various applications and related subjects at the frontiers are covered by comprehensive reviews by Quarkonium Working Group:

A-3. N. Brambilla *et al.* [Quarkonium Working Group Collaboration], “Heavy quarkonium physics,” hep-ph/0412158.

A-4. N. Brambilla, S. Eidelman, B. K. Heltsley, R. Vogt, G. T. Bodwin, E. Eichten, A. D. Frawley and A. B. Meyer *et al.*, “Heavy quarkonium: progress, puzzles, and opportunities,” *Eur. Phys. J. C* **71** (2011) 1534 [arXiv:1010.5827 [hep-ph]].

Acknowledgments

This lecture note is based on the lecture courses given at Rikkyo University, Kyoto University, Karlsruhe University and Nagoya University, during the years 2012–2014. The author is grateful to the members of the institutes of elementary particle and nuclear physics theory groups at these universities, for invitation and kind hospitality during the courses. In particular, the author would like to express his gratitude to Y. Takada, H. Suganuma, M. Steinhauser, J.H. Kühn and J. Hisano. This work was supported in part by Grant-in-Aid for scientific research No. 26400238 from MEXT, Japan.

A Formulas for Perturbative Series of $E_{\text{tot}}(r)$

In this appendix we collect some formulas necessary to compute the perturbative series of $E_{\text{tot}}(r)$, to facilitate the reading in Sec. 6. The formulas are given only for the case in which the masses of the quarks in internal loops are neglected, for the sake of simplicity.

We set the number of quark flavors to be n_f . The total energy is given by

$$E_{\text{tot}}(r) = 2m_{\text{pole}} + V_{\text{QCD}}(r). \quad (156)$$

The relation between the pole mass and the $\overline{\text{MS}}$ mass has been computed up to three loops in a full theory, which contains n_h heavy flavors (with equal masses) and n_l massless flavors in general. Setting $n_h = 1$ and rewriting the relation in terms of the coupling constant of the theory with n_f massless flavors only, we obtain

$$m_{\text{pole}} = \overline{m} \left\{ 1 + \frac{\alpha_s(\overline{m})}{\pi} d_0 + \left(\frac{\alpha_s(\overline{m})}{\pi} \right)^2 d_1 + \left(\frac{\alpha_s(\overline{m})}{\pi} \right)^3 d_2 + \left(\frac{\alpha_s(\overline{m})}{\pi} \right)^4 d_3 \right\}, \quad (157)$$

where $\overline{m} \equiv m_{\overline{\text{MS}}}(m_{\overline{\text{MS}}})$ denotes the $\overline{\text{MS}}$ mass renormalized at the $\overline{\text{MS}}$ -mass scale. The first three coefficients are given by

$$d_0 = \frac{4}{3}, \quad (158)$$

$$d_1 = \frac{307}{32} + \frac{\pi^2}{3} + \frac{\pi^2 \log 2}{9} - \frac{\zeta_3}{6} + n_f \left(-\frac{71}{144} - \frac{\pi^2}{18} \right) \\ \simeq 13.4434 - 1.04137 n_f, \quad (159)$$

$$d_2 = \frac{8462917}{93312} + \frac{652841 \pi^2}{38880} - \frac{695 \pi^4}{7776} - \frac{575 \pi^2 \log 2}{162} \\ - \frac{22 \pi^2 \log^2 2}{81} - \frac{55 \log^4 2}{162} - \frac{220 \text{Li}_4(\frac{1}{2})}{27} + \frac{58 \zeta_3}{27} - \frac{1439 \pi^2 \zeta_3}{432} + \frac{1975 \zeta_5}{216} \\ + n_f \left(-\frac{231847}{23328} - \frac{991 \pi^2}{648} + \frac{61 \pi^4}{1944} - \frac{11 \pi^2 \log 2}{81} + \frac{2 \pi^2 \log^2 2}{81} + \frac{\log^4 2}{81} \right. \\ \left. + \frac{8 \text{Li}_4(\frac{1}{2})}{27} - \frac{241 \zeta_3}{72} \right) + n_f^2 \left(\frac{2353}{23328} + \frac{13 \pi^2}{324} + \frac{7 \zeta_3}{54} \right) \\ \simeq 190.391 - 26.6551 n_f + 0.652691 n_f^2, \quad (160)$$

where $\zeta(z) = \sum_{n=1}^{\infty} 1/n^z$ denotes the Riemann zeta function, and $\zeta_3 = \zeta(3) = 1.2020\dots$, $\zeta_5 = \zeta(5) = 1.0369\dots$; $\text{Li}_n(x) = \sum_{k=1}^{\infty} \frac{x^k}{k^n}$ denotes the polylogarithm, and $\text{Li}_4(\frac{1}{2}) = 0.517479\dots$.

The fourth coefficient d_3 is not known exactly yet. Its value in the large- β_0 approximation is given by

$$d_3(\text{large-}\beta_0) = \frac{\beta_0^3}{64} \left(\frac{42979}{5184} + \frac{89\pi^2}{18} + \frac{71\pi^4}{120} + \frac{317\zeta_3}{12} \right) \\ \simeq 3046.29 - 553.872 n_f + 33.568 n_f^2 - 0.678141 n_f^3. \quad (161)$$

The QCD potential of the theory with n_f massless flavors only is given, up to $\mathcal{O}(\alpha_s^4)$ and $\mathcal{O}(\alpha_s^4 \log \alpha_s)$, by

$$V_{\text{QCD}}(r) = -C_F \frac{\alpha_s(\mu)}{r} \sum_{n=0}^3 P_n(L_r) \left(\frac{\alpha_s(\mu)}{4\pi} \right)^n, \quad (162)$$

where

$$L_r = \log(\mu^2 r^2) + 2\gamma_E, \quad (163)$$

and

$$P_0 = a_0, \quad P_1 = a_1 + a_0\beta_0 L_r, \quad P_2 = a_2 + (2a_1\beta_0 + a_0\beta_1)L_r + a_0\beta_0^2 \left(L_r^2 + \frac{\pi^2}{3} \right), \\ P_3 = \bar{a}_3 + \delta a_3^{\text{US}} + (3a_2\beta_0 + 2a_1\beta_1 + a_0\beta_2)L_r \\ + \left(3a_1\beta_0^2 + \frac{5}{2}a_0\beta_0\beta_1 \right) \left(L_r^2 + \frac{\pi^2}{3} \right) + a_0\beta_0^3 (L_r^3 + \pi^2 L_r + 16\zeta_3), \quad (164)$$

with

$$\delta a_3^{\text{US}} = \frac{16}{3}\pi^2 C_A^3 \left[\log(C_A \alpha_s(\mu)) + \gamma_E - \frac{5}{6} \right]; \quad C_A = 3. \quad (165)$$

The coefficients of the beta function β_n are given by

$$\beta_0 = 11 - \frac{2}{3}n_f, \quad \beta_1 = 102 - \frac{38}{3}n_f, \quad (166)$$

$$\beta_2 = \frac{2857}{2} - \frac{5033}{18}n_f + \frac{325}{54}n_f^2. \quad (167)$$

The constants a_n of the potential, not determined by the RG equation, are given by

$$a_0 = 1, \quad a_1 = \frac{31}{3} - \frac{10}{9}n_f \quad (168)$$

$$a_2 = \frac{4343}{18} + 36\pi^2 + 66\zeta_3 - \frac{9\pi^4}{4} - \left(\frac{1229}{27} + \frac{52\zeta_3}{3} \right) n_f + \frac{100}{81}n_f^2 \quad (169)$$

$$\simeq 456.749 - 66.3542 n_f + 1.23457 n_f^2, \quad (170)$$

$$\bar{a}_3 \simeq 13431.7 - 3289.91 n_f + 185.99 n_f^2 - 1.37174 n_f^3, \quad (171)$$

where presently \bar{a}_3 is known only numerically.

In order to achieve the renormalon cancellation between $2m_{\text{pole}}$ and $V_{\text{QCD}}(r)$ order by order in α_s expansion, we must use the same coupling constant $\alpha_s(\mu)$ in the series expansions of $2m_{\text{pole}}$ and $V_{\text{QCD}}(r)$. Therefore, $\alpha_s(\bar{m})$ is re-expressed in terms of $\alpha_s(\mu)$ as

$$\alpha_s(\bar{m}) = \alpha_s(\mu) \left\{ 1 + \frac{\beta_0 \log\left(\frac{\mu}{\bar{m}}\right)}{2} \left(\frac{\alpha_s(\mu)}{\pi}\right) + \left(\frac{\beta_1 \log\left(\frac{\mu}{\bar{m}}\right)}{8} + \frac{\beta_0^2 \log^2\left(\frac{\mu}{\bar{m}}\right)}{4}\right) \left(\frac{\alpha_s(\mu)}{\pi}\right)^2 + \left(\frac{\beta_2 \log\left(\frac{\mu}{\bar{m}}\right)}{32} + \frac{5\beta_0\beta_1 \log^2\left(\frac{\mu}{\bar{m}}\right)}{32} + \frac{\beta_0^3 \log^3\left(\frac{\mu}{\bar{m}}\right)}{8}\right) \left(\frac{\alpha_s(\mu)}{\pi}\right)^3 + \mathcal{O}(\alpha_s^4) \right\}, \quad (172)$$

which follows from the RG equation

$$\mu^2 \frac{d}{d\mu^2} \alpha_s(\mu) = -\alpha_s(\mu) \sum_{n=0}^{\infty} \beta_n \left(\frac{\alpha_s(\mu)}{4\pi}\right)^{n+1}. \quad (173)$$

Using Eqs. (157) and (172), we obtain the expansion of m_{pole} in terms of $\alpha_s(\mu)$,

$$m_{\text{pole}} = \bar{m} \times \left(1 + \sum_{n=1}^4 \tilde{d}_{n-1}(l_\mu) \left(\frac{\alpha_s(\mu)}{\pi}\right)^n \right) + \mathcal{O}(\alpha_s^5), \quad (174)$$

where the coefficients $\tilde{d}_n(l_\mu)$ are functions of $l_\mu = \log(\mu/\bar{m})$.

B Computation of $V_C(r)$

We show how to compute $V_C(r)$, given by eq. (96). We rotate the integral contour to imaginary axis in the complex q -plane. Setting $q = it/r$, we may rewrite

$$\begin{aligned} -\frac{2C_F}{\pi} \text{Im} \int_{C_1} dq \frac{e^{iqr}}{qr} \alpha_{\text{1L}}(q) &= -\frac{4C_F}{\beta_0 r} \text{Im} \int_0^\infty dt \frac{e^{-t}}{t \log(it/\Lambda_{\text{QCD}} r)} \\ &= -\frac{4C_F}{\beta_0 r} \left[-\pi + \text{Im} \int_0^\infty dt e^{-t} \log \left[\log(it/\Lambda_{\text{QCD}} r) \right] \right] \\ &= -\frac{4C_F}{\beta_0 r} \left[-\pi + \int_0^\infty dt e^{-t} \text{Im} \left[\log \left\{ \log t - \log(\Lambda_{\text{QCD}} r) + i\frac{\pi}{2} \right\} \right] \right], \quad (175) \end{aligned}$$

where we used integration by parts. Combining with $A/r = -4\pi C_F/(\beta_0 r)$, we obtain an expression of $V_C(r)$ given by an integral over t :

$$V_C(r) = -\frac{4C_F}{\beta_0 r} \int_0^\infty dt e^{-t} \text{Im} \left[\log \left\{ \log t - \log(\Lambda_{\text{QCD}} r) + i\frac{\pi}{2} \right\} \right]. \quad (176)$$

The integral is easily evaluated numerically for a given r .

To obtain asymptotic behaviors analytically we can expand $\text{Im} \log \left[\log t - \log(\Lambda_{\text{QCD}} r) + i\frac{\pi}{2} \right]$ in $\frac{1}{|\log(\Lambda_{\text{QCD}} r)|}$ before integration over t , which reduces to $\pi - \frac{\pi}{2|\log(\Lambda_{\text{QCD}} r)|}$ as $r \rightarrow \infty$, and to $\frac{\pi}{2|\log(\Lambda_{\text{QCD}} r)|}$ as $r \rightarrow 0$.

C Integration-by-regions Method and Relation to EFT

In this appendix, we explain the technique called asymptotic expansion of a diagram or integration by regions. This can be used to identify operators \mathcal{O}_i (effective interactions) in the Lagrangian of a Wilsonian EFT, eq. (80). At the same time the technique provides an efficient method for perturbative computations of Wilson coefficients $g_i(\mu_f)$.

Let us first explain the idea of the asymptotic expansion in a simplified example. We consider an integral

$$I(m; \epsilon) = \int_0^\infty dp \frac{p^\epsilon}{(p+m)(p+1)}. \quad (177)$$

It is a toy model imitating an integral in dimensional regularization. In fact, it is a one-parameter integral, imitating integral over the radial direction of a dimensionally-regulated integral, with $p^\epsilon dp$ representing a volume element; furthermore each propagator denominator is a linear function of p rather than a quadratic function. Suppose $m \ll 1$ is a small parameter and consider expanding I in m . Let us presume as if the integral region is divided into two regions $p < 1$ and $p > 1$, and expand the integrand in each region in a small parameter. Nevertheless, we restore the original integral region in each integral, as follows.

$$I = \int_0^\infty dp \underbrace{\frac{p^\epsilon}{p+m}(1-p+p^2+\dots)}_{p < 1} + \int_0^\infty dp \underbrace{\frac{p^\epsilon}{p+1} \frac{1}{p} \left(1 - \frac{m}{p} + \dots\right)}_{p > 1 \gg m}. \quad (178)$$

At a first glance, this seems to give a wrong result, since firstly we have extended each integral region to a region where the expansion is not justified, and secondly there would be a problem of double counting of region. Surprisingly, however, if we evaluate the individual terms of the above integrals and take their sum, it gives the correct expansion in m of the original integral I .

The reason can be understood as follows. Fig. 17 shows the analyticity of the integrand of eq. (177) in the complex p -plane: there are poles at $p = -1$ and $p = -m$; the origin is a branch point due to p^ϵ and the branch cut lies along the positive p -axis. The integral of p along the positive p -axis is equal to, up to a proportionality factor, an integral along the contour wrapping the branch cut. We may close the contour at negative infinity and deform the contour into the sum of two closed contours surrounding the two poles. (See Fig. 17: we deform the blue contour to the sum of the red contours.) Along the contour surrounding the pole at $-m$, it is justified to expand the integrand using the fact $|p| \approx m \ll 1$; this gives the integrand of the first term of eq. (178). After the expansion, the contour of the integral of each term of the expansion can be brought back to the original contour wrapping the branch cut along the positive p -axis. Similarly, along the contour surrounding the pole at -1 , we may expand the integrand using $|p| \approx 1 \gg m$, which gives the second term of eq. (178). Again, after the expansion, the

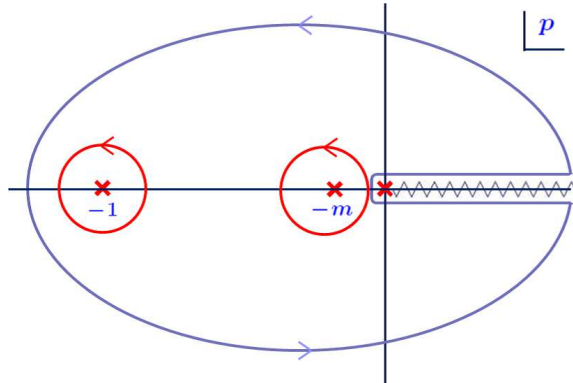


Figure 17: Analyticity of the integrand of eq. (177) in the complex p -plane. The blue contour can be deformed to the sum of the red contours.

integral contour can be brought back to the one surrounding the branch cut.* In this way, we obtain eq. (178).

Thus, for an integral that imitates a dimensionally-regulated one, we can expand the integral in a small parameter, without introducing a cut-off in the integral region. The important point in the above example is that the contribution from each of the scales $|p| \sim 1$ and $|p| \sim m$ is expressed by a contour integral surrounding the corresponding pole in the integrand (i.e., by the residue of each pole).

The method for the asymptotic expansion of a loop integral in dimensional regularization is the same: we divide the integral region into separate regions according to the scales contained in the integrand and expand the integrand in appropriate small parameters in respective regions; we nevertheless integrate individual terms of the expansions over the original integral region, namely, over the entire D -dimensional phase space for each loop integral.†

For illustration we consider the following two-loop integral in the case $p^2 \ll M^2$:

$$J(p^2, M^2) = \int d^D k d^D q \frac{1}{k^2(p-k)^2[(k-q)^2 + M^2]q^2(p-q)^2}. \quad (179)$$

The corresponding diagram is shown in Fig. 18, where the thick blue line represents a heavy particle with mass M and all other lines represent massless particles. We expand J in p^2/M^2 . The integral region of each loop integral is divided into two regions: high momentum region (H), $|k| > M$ or $|q| > M$, and low momentum region (L), $|k| < M$ or $|q| < M$. Hence, the whole integral region is divided into four regions: (H,H),(H,L),(L,H),(L,L). Of these (H,L) and (L,H) are the same due to the exchange symmetry between k and q . Fig. 19 shows how to perform the asymptotic expansion in each of these regions.

* In these manipulations, the value of ϵ in each term needs to be varied appropriately by analytical continuation into the domain where each integral is well defined.

† At the moment, the proof of this method using contour deformation as in the above toy model is missing, for general loop integrals in dimensional regularization. While it is likely that such an interpretation is possible generally, presently this type of proof is valid only in some selective cases. There exists a general proof based on different reasonings.

$$= \int d^D k d^D q \frac{1}{k^2(p-k)^2[(k-q)^2 + M^2] q^2(p-q)^2}$$

Figure 18: Two-loop diagram used to illustrate asymptotic expansion in p^2/M^2 . The thick blue line represents a propagator with mass M , while all other lines represent massless propagators.

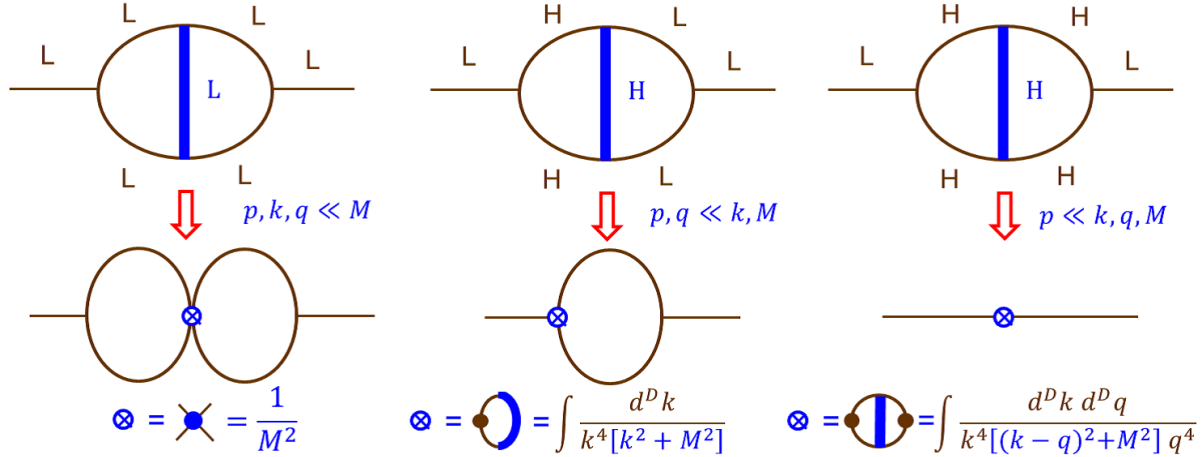


Figure 19: Diagrams showing procedure of the asymptotic expansion. The bottom line represent the Wilson coefficients of the leading-order effective vertices in respective regions.

In the region (L,L) we expand the massive propagator $1/[(k-q)^2 + M^2]$ in k and q . Each term represents an effective four-point vertex, where the leading vertex is given by a constant coupling $1/M^2$. This is depicted in the left-most part of the figure. Higher-order vertices are associated with powers of the factor $(k-q)^2/M^2$, which correspond to four-point interactions given by higher derivative operators.

In the region (H,L) we expand the propagator $1/(p-k)^2$ in p and the propagator $1/[(k-q)^2 + M^2]$ in q . In each term of the expansion, integral over k can be factorized, since p, q enter only the numerator of the integrand and can be pulled outside of the integral. This produces effective three-point vertices, which correspond to three-point interactions given by local operators. The leading term of this expansion is depicted in the middle part of the figure. Since high momenta flow through the k -loop, it is natural to expect that the loop effectively shrinks to a point.

In the region (H,H) we expand $1/(p-k)^2$ and $1/(p-q)^2$ in p . In this case, the whole integral over k and p can be factorized at each order of the expansion. Thus, each term can be regarded as an effective two-point interaction corresponding to a local operator. See the right-most part of the figure.

We may compute the same process in a low-energy EFT in which the massive particle has been integrated out. The asymptotic expansion of the diagram in the full theory obtained above can be interpreted as the computation in the EFT. The bottom-left

diagram in Fig. 19 represents a two-loop computation of this process in the EFT with an insertion of a four-point vertex, which is generated at tree-level of the full theory. The factor $1/M^2$ below the diagram represents the Wilson coefficient of the leading-order vertex in expansion in $1/M^2$. The bottom-middle diagram represents a one-loop computation of this process in the EFT with an insertion of a three-point vertex, which is generated at one-loop level in the full theory. The one-loop integral shown below the diagram represents the Wilson coefficient of the leading-order vertex in expansion in $1/M^2$. The bottom-right diagram represents a tree-level computation of this process in the EFT with an insertion of a two-point vertex, which is generated at two-loop level in the full theory. The corresponding leading-order Wilson coefficient is shown as a two-loop integral. Thus, the relevant operators and Wilson coefficients of EFT can be identified.

The Wilson coefficients, given by loop integrals in dimensional regularization, are particularly convenient in practical computations. They are homogeneous in a single dimensionful parameter M , which can be computed relatively easily. In contrast, if we adopt a cut-off regularization, usually it becomes much more difficult to evaluate the corresponding integrals (especially at higher loops), since more scales are involved.